Novel Preparation of Porous Alumina using Ice Particles as Pore-Forming Agents

Samantha G. Smith

Thesis submitted to the faculty of Virginia Polytechnic Institute and State University in partial fulfillment of the requirements for the degree of

Master of Science
in
Materials Science and Engineering

Gary Pickrell (chair)
Alex Aning
Carlos Suchicital

July 15, 2011
Blacksburg, Virginia

Keywords: porous ceramics, pore-forming agent, slip casting, ice

Novel Preparation of Porous Alumina using Ice Particles as Pore-Forming Agents

Samantha G. Smith

ABSTRACT

Porous ceramics have successfully been used in a wide variety of highly advanced applications. Current routes to porous ceramics are limited in the types of porosity they can create and no one process is flexible enough to create any desired structure. This study introduces the use of ice particles as pore forming agents to fabricate porous materials. This novel method possesses several advantages over current industrial techniques including environmental friendliness, low cost, and flexibility in size and shape of resulting pores. Porous ceramic structures were created by adding preformed ice particles to an alumina slurry which was quickly frozen, air dried, and then sintered. Porosity was characterized using Scanning Electron Microscopy (SEM), Archimedes measurements, and gas sorption techniques. Small spherical pores were successfully created in the 20-200μm range and larger spherical pores were also created in the 2-3 mm range. Amount of porosity was controlled through specifying the amount of ice added to the ceramic slurry. Samples were prepared with porosity levels ranging from 30-75%. As a completely new process, these initial results are quite promising and further development will allow for even greater morphology control.

Acknowledgements

First, I would like to thank my parents for their continuous love and support. I am incredibly lucky to have such amazing parents and I would not be where I am today without them. Thanks to my sister, Michelle, for being my Chipotle partner whenever I needed it. I am especially thankful for my boyfriend, Brian. I could not have done this without his constant support and encouragement, even from the other side of the country.

I would like to acknowledge the Materials Science and Engineering Department at Virginia Tech for providing much of the equipment used to complete this work. Thanks to the Institute for Critical Technology and Applied Sciences (ICTAS) and Steve McCartney for assistance with and use of the SEM. I am extremely thankful to Dr. Pickrell for his support and guidance throughout my graduate studies. He has been an outstanding advisor and I truly appreciate the opportunity to get involved in this exciting project. Special thanks go to Brian Scott, from Dr. Pickrells group, for offering his time and his great ideas to help me finish up this project. I would also like to acknowledge my committee members Dr. Alex Aning and Dr. Carlos Suchicital for their invaluable advice.

Table of Contents

List of Figures

List of Tables

Chapter 1. Introduction

The field of porous ceramics has been growing rapidly as these materials have been successfully utilized in increasingly diverse and advanced technological applications. These applications include molten metal filters[1], hot gas filters [2], catalytic supports [3], thermal insulation [4], lightweight structural components [5], and bone regenerations scaffolds [6], just to name a few. Each application requires a unique set of pore structures and some of the more high tech applications can require pore structures that are quite complex. For example, Takahashi et al. introduced a double-layered porous alumina filter, which helps to reduce the pressure drop seen across the filter [7]. The microstructure of the double-layered pore structure is seen to the right in Figure 1. The amount of open and closed porosity, pore size and shape, pore uniformity, and degree of pore interconnectivity all play crucial roles in determining the degree of success of a porous component in its intended application.

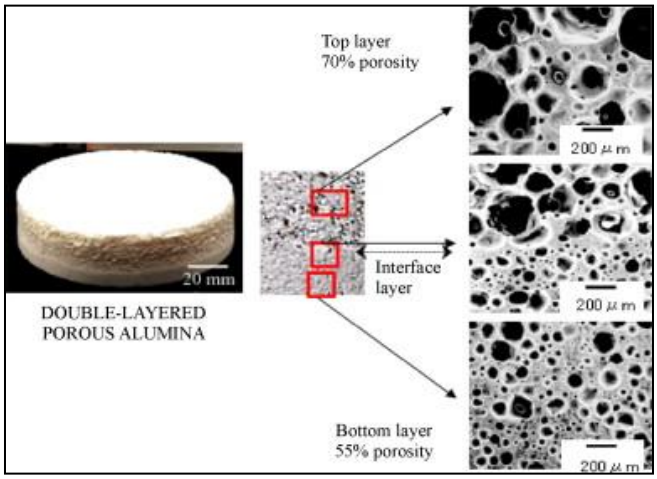

Figure 1 Complex double-layered pore structure for filtration applications [7]

Specific pore requirements are met through the selection and control of an appropriate ceramic processing method. Several different methods are used to manufacture porous materials, each with its own set of advantages and disadvantages. The majority of processing methods that currently exist are limited in the types of pores they can produce. Freeze-casting, for example, an environmentally friendly technique; however, this method is only able to make unidirectionally aligned cylindrical pores. An ideal processing route to porous ceramics would be able to create any type of porous microstructure within any system. It would also be easy to control, cost effective, easily performed in a manufacturing environment, and environmentally friendly. Such a technique does not currently exist, although extensive research is ongoing to identify one.

The purpose of the present study is to introduce and prove the feasibility of a novel processing route to porous materials using ice particles as a pore-forming agent (PFA) or a pore template. Ice particles can act as a pore holder when introduced to a ceramic slip. The structure can be set through freezing and a simple drying process removes the ice, leaving a void in its place. This method has the potential to meet all of the above described ideal requirements: flexibility in obtainable pore microstructures, cost effectiveness, environmental friendliness, and ability to be performed in a manufacturing environment. Flexibility in pore size and shape is easily obtained with this method. Ice particles can be created ahead of time to the exact size and shape of the desired pores within the final structure. Spherical ice particles in a wide range of sizes can be created to form uniform spherical pores in a ceramic component. If open directionally aligned tube shaped pores are desired, columnar ice crystals can be grown and held in place while a ceramic slip is poured around them. Once the structure is set and the part is dried, the directionally aligned tubular voids will be present where the ice crystals once existed. Higher degrees of porosity can be obtained by increasing the amount of ice introduced to the ceramic slip.

Ice particles have considerable advantages over typical templating materials. Most often, organic PFA's are chosen to hold the place of pores within a slip. Many different kinds of organic PFAs have been used to make porous materials including spherical polystyrene beads [8], organic polymer sponges [9], biological agents [10], poppy seeds [11], wheat flour [12], graphite [13] and polyurethane foam [14]. These organics must be burned out for removal from the system, and organic burnout poses several environmental concerns, such as the release of volatile organic components (VOCs) into the atmosphere. Ice, on the other hand, has no known negative environmental effects. Secondly, many of the organics that have been used as PFAs are limited in size and shape. Poppy seeds, for example, which were used as a PFA in a study by Gregorvia et al [11], only come in one size. This is not a limitation for a system which uses ice particles as a PFA.

Ice particles have potential cost advantages over other PFA materials in a manufacturing environment. The elimination of an additional burn-out schedule saves time and money. Ice particles can easily be made in house as needed, eliminating the need to store PFAs in a warehouse before being used.

While porous ceramics are the focus of this study, this process also has the potential to be used to create porous metallic components via a metallic powder processing method. Because this is a new technique, many options must be investigated to find the ideal processing method. In this study, different ice shapes and sizes, ice volumes, setting and drying techniques, and sintering schedules are explored. The goal is to introduce this method as a feasible processing route to porous ceramics and to identify the boundaries of the process. It is expected that pore size, shape, interconnectivity, and percent porosity will be easily controlled using this novel fabrication technique.

Chapter 2. Literature Review

2.1 Porous Ceramics

Recent interest in porous ceramics has been fueled by the successful integration of these materials into many advanced technological applications. Porous catalytic supports are employed in micro-scale combustors for power generation [15]. Highly developed porous ceramic membranes function as micro-filters in extremely corrosive and high temperature environments [16]. Pores introduced in piezoceramics make these materials suitable for underwater sonar detectors and ultrasonic imaging applications [17]. Porous ceramics have also been widely used in the biomedical field as bone scaffolds and bone replacements [18].

Alumina is very well known for its excellent wear properties, making porous alumina components highly favorable among many different types of applications. Within the biomaterials community, porous alumina components are extremely desirable in bone tissue engineering. In bone regeneration applications, the alumina must have relatively large pores (>100 μm) that are well interconnected to allow for adequate bone in growth [19]. Current work within this field is attempting to improve the compressive strengths of these highly porous ceramic parts.

2.2 Ceramic Processing Methods

Porous ceramics may be categorized into one of four different structure types: tangle fiber networks, closed cell structures, open cell structures, and membranes [20]. Depending on the type of application, a ceramic component will need any one of these structures. For example, in many filter applications, ceramics are desired with unidirectional cylindrical pores that are uniform in size and shape. These types of pores will allow for high permeability through the filter and they will provide high overall strength for the filter. The ability to obtain these different structures depends entirely on the way the ceramic is processed and this has been a topic of much interest to the scientific community [9].

Porous ceramics can be synthesized via several different routes, each with its own list of advantages and disadvantages. Ceramic processing typically begins with the formation of a green body from a ceramic starting powder. The powder can be processed via a dry method or a wet method, where the powder is introduced to a liquid. Some commonly used methods include gel-casting, tape casting, injection molding, in-situ decomposition, and freeze-casting, among several others [21, 22]. The methods described below are most closely related to the method introduced in this study, the use of ice particles as a pore-forming agent.

2.2.1 Dry Powder Partial Sintering

A simple way to create a porous ceramic is through partially sintering a compacted dry ceramic powder. Pores will form between the powder particles as necking occurs during sintering, and the amount of porosity in the final product is determined by the sintering temperature and time [22]. As long as the compact is not fully sintered, porosity will remain in the component. Higher levels of porosity can be obtained when green compacts are formed by die-pressing a mixture of ceramic powder and organic additive [23]. The ideal organic additive is one which will easily decompose at a relatively low temperature. When the compact is sintered, the organic additive will burn out, leaving behind a pore in its place. The addition of more organic additive to the compact will result in more porosity as well as higher levels of pore interconnectivity.

2.2.2 Slip Casting- Sacrificial Templating Technique

Slip casting is a wet ceramic forming process that is commonly used in commercial industry to fabricate both porous and compact ceramic articles [24]. In the slip casting method, a powder ceramic is dispersed in an aqueous solution to create a ceramic slurry or a slip. A dispersant is often added to the slurry to counteract the Van der Waals forces between powder particles which tend to cause powder agglomeration within the aqueous suspension [25]. The ceramic slip is then poured into a porous mold which uses capillary action to remove the solution from the powder slip, leaving behind a green body

mold. The green body is then fired to impart strength on the cast ceramic part [26]. Figure 2 shows the typical steps used in the slip casting method.

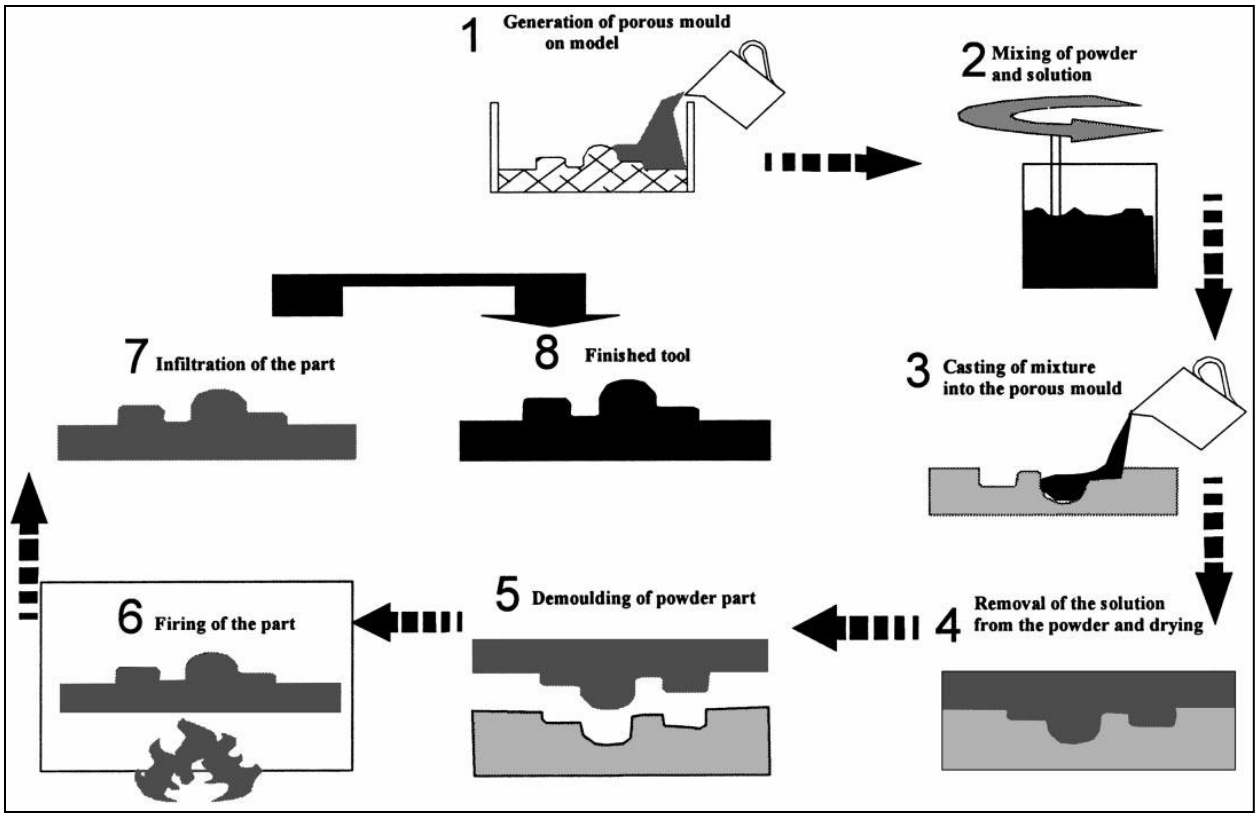

Figure 2 Slip-casting processing steps [26]

When a porous component is desired, pore-forming agents are also added to the slip before being poured into the mold. Once the slip is dried and cast within the mold, the pore-forming agent (typically an organic) is burned off, leaving behind a pore of identical size and shape. Several different materials have been used as pore forming agents in the slip casting method, including spherical polystyrene beads [8], organic polymer sponges [9], biological agents [10], poppy seeds [11], wheat flour [12], graphite [13], and polyurethane foam [14]. The pores are controlled by the type and amount of pore-forming agent introduced to the slip during preparation. Slip casting is a relatively simple and inexpensive method for forming porous ceramics.

2.2.3 Polymeric Sponge Templating- Replica Technique

Porous ceramics may also be formed using a pre-existing polymer sponge as a template. An organic polymer sponge (often polyurethane) is selected with the same pore size and structure that is desired in the final ceramic component. The sponge is coated with a ceramic slurry, such that the ceramic forms an even and homogenous layer around the sponge [14]. The coated part is then heated up to decompose and burn out the organic polymer sponge. Heat is then further increased to sinter the remaining ceramic structure [20]. The final ceramic component is identical to its polymer sponge counterpart except for its slightly smaller pore sizes, an unavoidable effect of the coating process.

Sponge templating is commonly used in the ceramic processing industry because of its simplicity. As long as a polymer sponge can be made with the correct pore structure, ceramic copies can be made. This preparation method is limited to creating open-cell structures only. Because the ceramic slurry must be able to reach all parts of the structure, closed porosity cannot be achieved.

2.2.4 Freeze Casting

Freeze casting was first introduced to the scientific community in 1992 and has since been widely studied as an economical and environmentally friendly route to produce porous ceramic matrix composites [27-33]. In this technique, a ceramic slip with a low solid content is poured into a mold and subsequently frozen. The solidification of the slip suspension forms dendritic ice crystals which push aside ceramic particles and form long ice channels throughout the sample [34]. The entire structure is set by the frozen liquid which is then sublimated by freeze drying. Once dried, the remaining ceramic green body structure has open pore channels existing where the ice crystals had originally grown. The porosity within these structures strongly depends on the growth of ice crystals and is typically controlled by the solid loading within the slip and the rate of freezing of the sample [32, 35].

This forming technique is favorable because of its environmental friendliness as compared to other methods which use an organic pore template. Freeze casting is particularly effective in creating structures with unidirectionally aligned pores, as the slurry is frozen from one direction. The major

drawback is the fact that this process is severely limited because it is only able to create one type of pore. Because of the nature of the ice crystal growth in the suspension, freeze casting methods are limited to producing ceramic articles with a high amount of open, tubular shaped porosity only. The microstructure of a typical porous article prepared via freeze-casting is shown below in Figure 3.

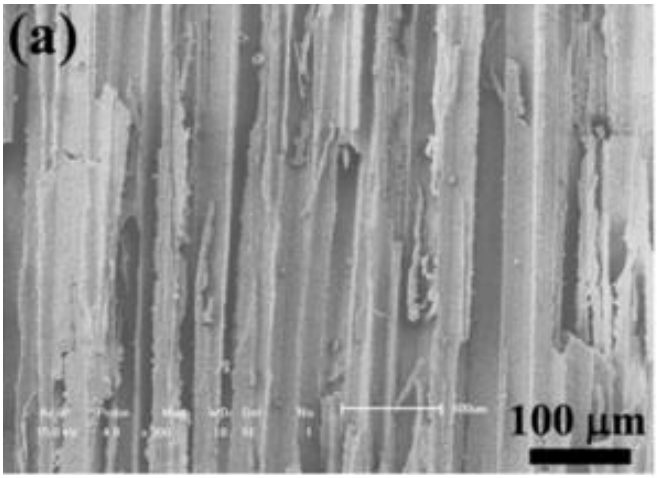

Figure 3 Unidirectionally aligned pore channels within a Yttria Stabilized Zirconia (YSZ) sample prepared by freeze-casting [33]

It is not possible to create closed pores using freeze-casting because of the nature of ice growth through the sample. While the cylindrical tube shapes have been found to be quite useful in bone tissue engineering applications [19, 36], this type of structure is not useful when it comes to most other applications, such as in heat insulation components. Several papers report on the ability to control pore morphology using the freeze casting method [28-31, 37, 38] however this comes at the expense of severely complicating the freeze casting process. The changes made focus on control of the dendritic features that form off of the tubes. The resulting pores are still unidirectionally aligned channels running throughout the sample.

2.2.5 Gel-Casting

Gel-casting is a method that utilizes the binding ability of a polymer to set structures and improve the mechanical strength of green bodies. Gel-casting has been widely used in the preparation of porous ceramics and is quite successful [39-41]. First, a ceramic powder solution is well dispersed within a monomer solution. Pores may be introduced to this ceramic/monomer solution via sacrificial templating or the slurry can be used to coat a polymeric sponge for the replica technique. Dense structures may also be obtained via gel-casting wherein no pore forming agents would be introduced to the solution. When the desired structure is obtained, polymerization or gelling is promoted to set the structure by trapping the ceramic particles within the rigid polymeric network [42]. The resulting green body will have improved mechanical strength and can even be machined to obtain a specific part size. Gel-casting is also highly favorable because it is a near-net shape process for forming porous components. The added strength from the polymerized network prevents collapse of the green body during drying. Figure 4 presents an excellent flowchart of the gel-casting process [39].

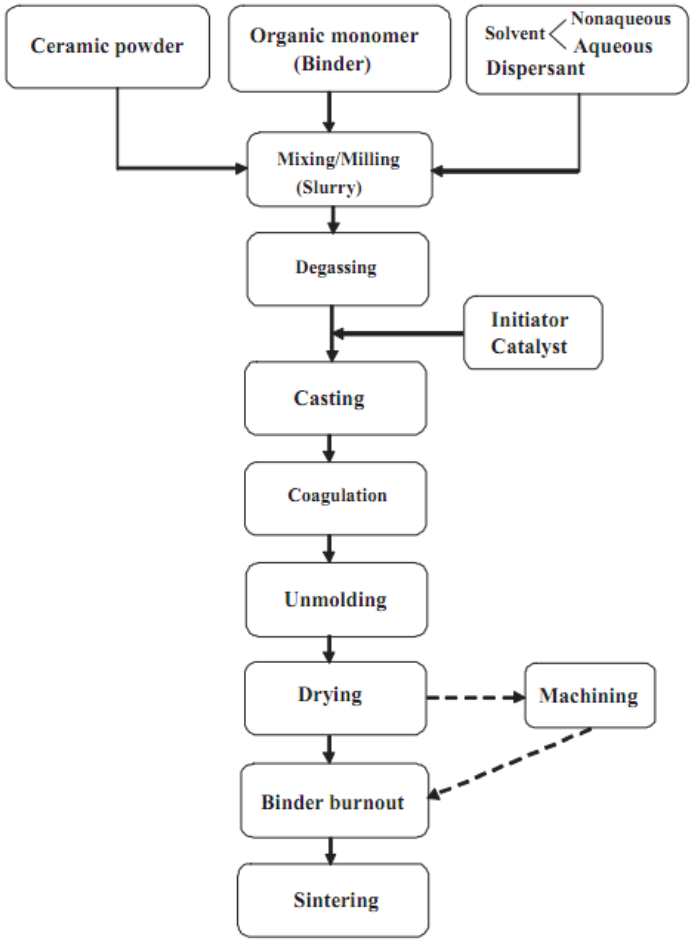

Figure 4 Flowchart of the gel-casting process [39]

When gel-casting was first introduced to the scientific community in the early 1990's, acrylamide was most often used as the binding polymer. Acrylamide was later realized to be a neurotoxin, and so

efforts turned toward developing more natural based cross-linking polymers [43]. Agarose is a environmentally friendly biopolymer that is actually derived from algae and it requires changes in temperature to activate hydrogen bonds between monomers, forming a gel [39]. Gelling within a solution of agarose occurs when cooled below 45˚C. When the gelled solution is reheated above 80˚C, the non-covalent hydrogen bonds and electrostatic interactions will break, leaving the monomer units behind. Potoczek et al successfully created porous alumina components via gel-casting with agarose [44]. Pores were introduced via a foaming method. A 4 wt% solution of agarose monomers was heated to 90˚C and then carefully kept around 60-65˚C before being introduced to the ceramic slurry to ensure the cross-linking step did not occur before pores were introduced. The agarose solution was added to an alumina slurry solution in varying amounts such that the final amount of agarose ranged anywhere from 0.25 to 1.00 wt %.

Ewais et al also prepared ceramic slurries using agarose as a gelling agent [45]. Agarose was successfully removed from the samples using the following heating schedule: ramp up 3˚C/min to 500˚C, dwell for 3 hours at 500˚C, and cooling back down to room temperature at a rate of 3˚C/min.

2.3 Drying

Drying is very critical in the preparation of ceramic materials and often times is the longest processing step [46]. The most commonly used drying techniques currently used include air drying and microwave drying [47]. When articles are not uniformly dried, cracking, warpage, bending, and shrinkage can occur which can make a component useless [48]. As water is removed from a wet green body, ceramic particles are free to move and fill the space once held by water. In some cases the ceramic particles will move until they are in contact with one another. Stresses present from the movement of ceramic particles can induce micro-and macro cracking within the ceramic component. Many studies have focused on altering the drying process to ensure the shape of a ceramic part does not change throughout processing, also called a near net-shape process [46, 49-52]. Gel-casting, as described above

in section 2.2.5, is a near net-shape forming process. The polymerization of the gel within the slurry provides strength to a green body and prevents shrinkage and cracks in a ceramic component [53].

2.4 Sintering

Sintering is an extremely crucial step in ceramic powder processing. During solid-state sintering, particle transport is driven by free energy reduction and results in densification, pore annihilation, and grain growth within the powder compact [54]. The sintering of a powder compact progresses through three stages: initial, intermediate, and final. During the initial stage, necking takes place at a relatively high rate due to the large curvature of the particles. It is important to note that during the initial stage, necking occurs via six different competing mechanisms, some which lead to densification, or shrinkage, and others which lead to coarsening, or a growth of the neck without shrinkage. These mechanisms are listed below in Table 1 [54].

Table 1 Particle transport mechanisms during the initial stages of solid-state sintering [54]

Mechanism Number	Transport Path	Source of Matter	Sink of Matter
1	Surface Diffusion	Surface	Neck
2	Lattice Diffusion	Surface	Neck
3	Vapor Transport	Surface	Neck
4	Boundary Diffusion	Grain Boundary	Neck
5	Lattice Diffusion	Grain Boundary	Neck
6	Lattice Diffusion	Dislocation	Neck

For example, the transport of material from the particle surface to the neck will not decrease the distance between two particle centers and so, will not cause shrinkage. However, transport of material from the particle volume or from a grain boundary to the neck will decrease the distance between two particle centers, resulting in densification [54]. Mechanisms that result in densification are promoted at higher temperatures; therefore, densification is more commonly seen at higher sintering temperatures.

During the intermediate stages of sintering, pore channels are formed at the junction of three grains and the channels begin to narrow. The powder curvature at the neck has diminished, slowing down

the rate of particle transport. At the final stage of sintering, pores are isolated from one another. This transformation is displayed below in Figure 5 from a study by Lame et al. [55]. The location of the pores is also very important in determining the final amount of porosity after sintering. A pore that is located on the grain boundary can be eliminated by boundary diffusion and lattice diffusion while a pore within a grain can only be eliminated by lattice diffusion. Because lattice diffusion is typically much slower than other transport mechanisms, pores within a grain are much harder to eliminate [54].

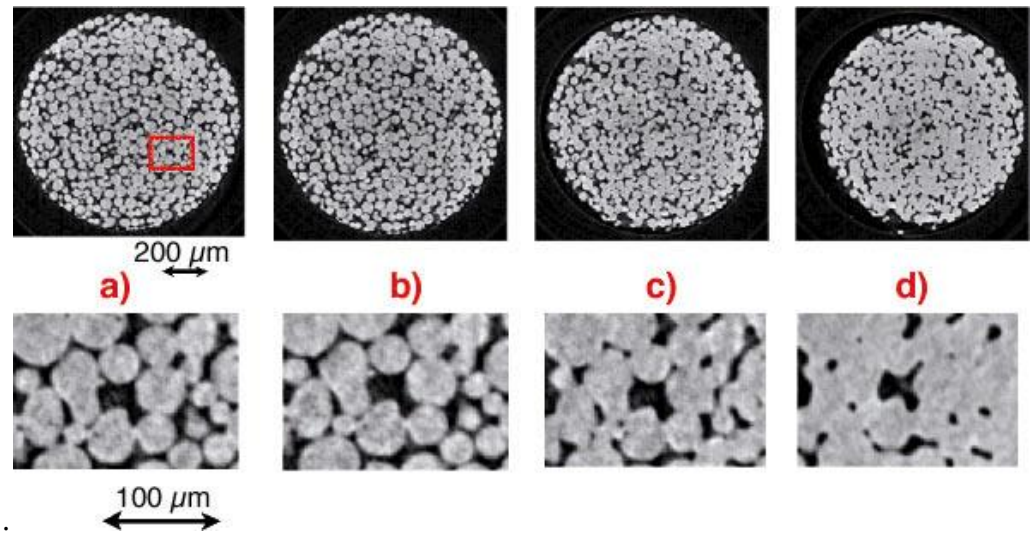

Figure 5 Stages of solid-state sintering over time: a) initial b) intermediate c) late intermediate and d) final [55]

2.5 Porosity Resulting from Pore-Forming Agents

When a pore-forming agent is used to create porosity within a body, it is important to understand how the volume of PFA in the green body will translate to volume of porosity within the final sintered ceramic body. The X_{pf} parameter, defined by Slamovich and Lange, allows for the comparison between volume of PFA added to a green body and porosity of a sintered ceramic part [56]. This parameter takes into account the volume of PFA with respect to the overall volume of solids, ϕ, as well as the packing

density of the ceramic particles in the green body without any PFA added, ρc. The calculation for X_{pf} is shown below in Equation 1[56].

$$X_{pf} = \frac{\phi(\rho c)}{1-\phi+(\rho c)\phi} \qquad \text{Eq. 1}$$

When the pores left by the PFAs are sufficiently large, Slamovich and Lange assumed that the pores will shrink by the same amount that the surrounding ceramic matrix will shrink. Under this assumption, X_{pf} will be equal to the amount of porosity found in the final, fully densified sintered body [57]. If the body is not fully densified, X_{pf} will be smaller than the total porosity in the sintered body and the difference is porosity that results from partial sintering of the powder particles. In other words, the porosity found in a sample depends on the volume fraction of PFA added to the green body X_{pf} as well as the time and temperature of sintering [57].

Chapter 3. Materials and Methods

In general, the following procedure was used: alumina slurries were mixed with ice, poured into a mold and set, removed from the mold, dried, and sintered. Variations were systematically studied for most steps in the process. Two different ceramic systems were used: one alumina system without a binder and one alumina system with a biopolymer gelling agent. Three different types of ice particles were tested, varying in shape, size, and uniformity. The amount of ice introduced to the ceramic slurry was varied. Structures were set by either freezing or cooling to room temperature, depending on the presence of binder in the slurry. Finally, sintering temperatures were varied from 1300˚C to 1600˚C. Samples were analyzed to determine the effect of the process variations on the pore volumes, pore sizes, and pore microstructures. Characterization of the fired samples was performed using scanning electron microscopy (SEM), optical microscopy, Archimedes' measurements, and gas adsorption. Optical microscopy was also used to characterize the size and shape of the ice particles introduced to the ceramic slurries.

3.1 Ice Particle Fabrication

In order to illustrate the flexibility of this process, pores were made using ice particles of different shapes and sizes. This way it would be possible to see if a change in the shape of ice particle causes a change in the shape of the resulting pore. Three kinds of ice particles, differing in size, shape, and uniformity were made for this study.

3.1.1 Crushed Ice Particles

Crushed ice particles were made using a commercial blender. The blender selected was a NINJA (shown in Figure 6), which is specifically designed to crush ice. Pre-frozen ice cubes from an ice tray were added to the blender and crushed until the blender could no longer make the ice any smaller. The

crushed ice was expected to be random in both size and shape due to the chaotic and random nature of the blending process.

3.1.2 Spherical Ice Particles

Figure 6 Ninja blender used to crush ice and mix slurries

Ceramic structures with spherical pores are often desired in many structural based applications because these types of pores allow for better mechanical strength within the ceramic component. To create ice particles with more shape uniformity than those created in the blending process, spherical ice particles were made by hand, using liquid nitrogen. Two methods were used to introduce water droplets to a dewar of liquid nitrogen, creating ice particles of two different sizes. A nozzle from a spray bottle was used as a water atomizer to create smaller spherical ice particles (referred to as smaller spherical ice). An eye dropper was utilized to make significantly larger spherical ice particles (referred to as larger spherical ice). When water droplets were introduced to the liquid nitrogen, they quickly froze and sank to the bottom of the dewar because ice is more dense than liquid nitrogen. After the desired amount of ice had been made, the ice particles collected at the bottom of the dewar were scooped out to be added to the ceramic slurry.

Particular care had to be taken during the spraying process. If sprayed too quickly, the ice particles tended to agglomerate together at the surface of the liquid nitrogen dewar. Instead of forming small ice particles, the water droplets collected together and formed large ice chunks before freezing and sinking to the bottom of the dewar. To avoid this problem, the nozzle was sprayed once every 3 seconds. This amount of time was sufficient to allow all of the sprayed water droplets to completely freeze and sink to the bottom before more water droplets were added. Table 2 below summaries the types of ice

particles made for this experiment and their expected properties. Ice properties were later confirmed using optical microscopy techniques.

Table 2 Ice particles made and expected ice properties			
Ice Type	Made From	Shape	Size
1	Blender	Crushed	Random
2	Atomizer and liquid nitrogen	Spherical	Small
3	Dropper and liquid nitrogen	Spherical	Large

3.2 Ceramic Slurry Preparation

Alumina systems were prepared using commercially available α-Al_2O_3 powder (99.9% purity, <1.0 micron, Alfa Aesar). Two different slurry systems were prepared to determine the effect of using an organic binder in the system.

3.2.1 Alumina System without a Binder

Slips were prepared by adding alumina powder to deionized water until a thick slurry was obtained. Slurries must be quite viscous in order to suspend the ice particles while the ceramic structure is being set. The desired amount of powder was weighed out on a scale. Any visible powder agglomerates were manually crushed with a spatula and the powder was then mixed dry in the blender to further remove any clumps. Suspensions were prepared with an alumina solid loading of approximately 53 wt% to create a sufficiently thick ceramic slip. The appropriate amount of water was then added to the blender and blended for several seconds to ensure complete mixing of the slip. Slips were visually inspected to ensure complete mixing was achieved.

3.2.2 Alumina System with Agarose Gelling Binder

Commercially available agarose powder (Fisher Scientific, Low EEO/multipurpose grade) was used to prepare a 4 wt% agarose solution in deionized water. The agarose solution was heated in a flask on a hotplate to 90˚C for 20 minutes to allow for complete breakdown of the binder into a monomer

solution. A stir bar continually stirred the agarose solution while being heated. The solution was then maintained at a temperature of 60-65˚C to ensure gelling did not occur. The alumina slurry for this system was prepared in the same manner as the slurry without binder (described in 3.2.1); however, the alumina solid loading in these slurries was initially prepared at 64 wt%. This way, when the agarose solution was added to the alumina slurry, a final alumina solid loading of 53 wt% was obtained, exactly the same as in samples without binder. The 4 wt% agarose solution was added such that all final agarose/alumina systems contained 53 wt% alumina and 0.75 wt % agarose binder.

3.3 Introduction of Ice to the Ceramic Slurry

Ice particles were introduced to the alumina and alumina/agarose systems to create alumina/ice mixtures. Variations were made in the type of ice that was added (crushed, small spherical, or large spherical) as well as the amount of ice added by volume percent (0, 43, 56, or 75). Alumina samples were prepared with 0 volume percent ice, 43 volume percent crushed and large spherical ice, and 43, 56, and 75 volume percent small spherical ice. The alumina/agarose systems were prepared with 0 volume percent ice, and 43, 56, and 75 volume percent small spherical ice.

3.3.1 Alumina System without a Binder

Ice was introduced to the slip in the blender. The plain alumina system without a gelling agent was prepared with all three types of ice particles : crushed, small spherical, and large spherical. In the case of the crushed ice, large ice cubes were added and crushed while being blended in with the ceramic slurry. Because the spherical ice particles were made ahead of time, these were added to the blender and blended with the ceramic slurry to mix. The spherical ice particles were already small enough that they were not significantly crushed any further when mixed in the blender.

The amount of ice added to the blender depended on the desired amount of porosity within the final part. Higher ice-to-slip volume ratios were used to obtain higher amounts of porosity. For crushed ice systems, ice volume was measured by adding the appropriate number of large ice cubes,

understanding that each ice cube had a volume of approximately 15 cc. Slurries prepared with crushed ice contained 43 volume percent ice. The desired volume of spherical ice added was obtained by weighing the ice particles before adding them to the slip. Slurries with 43 volume percent ice were prepared using both the small and large ice particles. To determine the maximum amount of porosity that can be achieved in the small spherical ice particle system, samples were made with 55 as well as 75 volume percent ice. One control group of samples was also prepared without the addition of ice. These samples were intended to determine the amount of porosity resulting from other aspects of processing, such as the loose packing nature of the powder particles and partial sintering.

Ceramic/ice mixtures were then scraped out of the blender into small circular aluminum dishes using a spatula. The dishes were filled to the top with the ceramic ice mixture to allow for comparisons in volume shrinkage during later stages of processing. The aluminum dish had a diameter of 7 cm and a height of 1.25cm. The mixture was carefully added to avoid the introduction of any air to the sample. If air pockets appeared, they were pushed out with the spatula. Porous molds were not used here because the structure of the sample needed to be set before any water was removed. Samples were frozen one of two ways. A majority of samples were placed in a freezer at -5˚C overnight to freeze. A few samples were frozen more quickly by introducing them to cryogenic temperatures immediately after being poured in the aluminum dish.

3.3.2 Alumina System with Agarose Gelling Binder

Alumina agarose systems were prepared using 43, 56, and 75 volume percent small spherical ice. For this system, ice was added to the system immediately after the agarose solution was poured into the blender as described above. The ice and slurry were blended as quickly as possible and immediately scooped into the aluminum dish mold. The mold was only needed to form the desired shape of the green body. The aluminum dish was peeled off of the sample after molding and the sample was placed on the lab bench to set and dry. These samples need not be frozen to allow the structure to set because agarose will polymerize when left at room temperature. An alumina agarose system without any ice was also

made as a control sample. Table 3 summarizes each of the different ceramic slurry and ice mixtures made for this experiment.

Table 3 Alumina/ice mixtures prepared

Mixture	Ceramic System	Ceramic Loading in Slurry (wt%)	Ice Type	Volume Percent Ice
AC	Alumina	50.0	None	0
A1	Alumina	53.1	Crushed	43.8
A2	Alumina	53.1	Small Spherical	43.8
A3	Alumina	55.8	Small Spherical	56.2
A4	Alumina	57.1	Small Spherical	75.1
A5	Alumina	53.1	Large Spherical	43.8
A6	Alumina/Agarose	52.3	Small Spherical	0
A7	Alumina/Agarose	52.9	Small Spherical	44.3
A8	Alumina/Agarose	52.9	Small Spherical	56.8
A9	Alumina/Agarose	52.9	Small Spherical	75.2

3.4 Drying and Agarose Burnout

3.4.1 Alumina Systems without a Binder

Frozen samples were removed from the freezer and the aluminum dish mold was peeled off leaving behind the circular ceramic sample. The samples were left overnight on the lab bench to dry in room conditions. Once all ice had melted out and the samples were relatively dry to the touch, they were moved to a furnace for further drying. Complete drying was achieved by heating samples in a small Barnstead Thermolyte furnace for 12 hours at 150˚C. The dried ceramic parts were

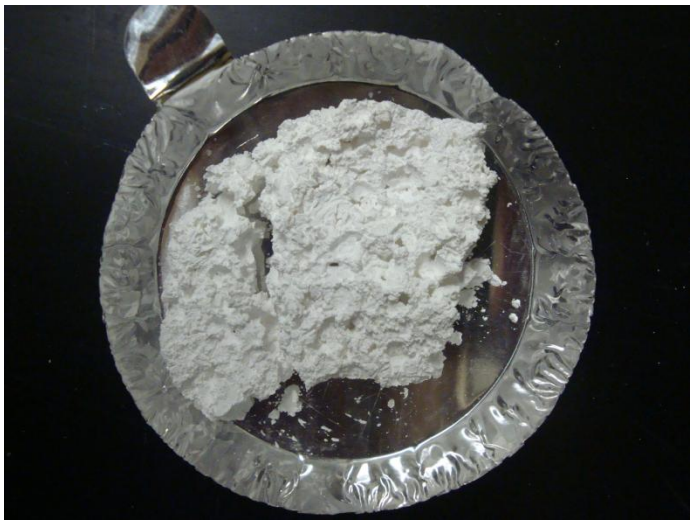

Figure 7 Dried green body

quite brittle and difficult to handle. Therefore, tremendous care was taken when moving the samples from the lab bench to the furnace. Figure 7 depicts a dried green body in the aluminum dish used as a mold.

3.4.2 Alumina System with Agarose Gelling Binder

Alumina agarose samples were removed from the aluminum mold immediately after being poured from the blender. The samples were left on the lab bench overnight for an initial drying. Further drying and removal of the organic agarose were achieved in the Barnstead Thermolyte furnace. A heating rate of 3˚C/min was used up to 500˚C. The samples were kept at 500˚C for 3 hours and then cooled back down to room temperature at the same rate of 3˚C/min.

3.5 Sintering

Samples were fired in air using a Deltech Inc. tube furnace (shown in Figure8). A heating rate of 1.5˚C/ min was used followed by a 2 hour dwell at 1300˚C, 1500˚C, or 1600˚C. After the dwell, samples were cooled back to room temperature at 1.5˚C/ min. Alumina samples with 43 volume percent ice (either spherical or crushed) were sintered at all three temperatures. Alumina samples without any ice were sintered at 1300˚C and 1500˚C. All other samples, including samples with agarose, were sintered at 1500˚C only. Table 4 summarizes the matrix of the 11 types of alumina samples prepared and table 5 summarizes the matrix of 4 alumina/agarose samples prepared. The astericks seen in Table 4 indicate those samples were frozen both in a freezer and in liquid nitrogen (as described in section 3.3.1).

Figure 8 DelTech Inc. tube furnace

Table 4 Summary of Alumina Samples Prepared						
Sintering Temperature (˚C)	No Ice	Crushed Ice	Small Spherical			Large Spherical
	0 vol %	43 vol %	43 vol %	56 vol %	75 vol %	43 vol %
1300	X	X	X*			
1500	X	X	X*	X	X	X
1600		X	X*			
*slurries were frozen both in a freezer and in liquid nitrogen						

Table 5 Summary of Alumina/Agarose Samples Prepared				
Sintering Temperature (˚C)	No Ice	Small Spherical		
	0 vol %	43 vol %	56 vol %	75 vol %
1300				
1500	X	X	X	X
1600				

3.6 Characterization

Fired samples were characterized to understand the effect of ice type and amount, ceramic system, freezing method, and sintering temperature on volume shrinkage, porosity, and microstructure. Samples were measured to determine the amount of shrinkage occurring during processing. Archimedes' principle was utilized to qualitatively understand the amount of total, open, and closed porosity within samples. SEM and optical microscopy were used to quantitatively assess pore size and qualitatively review pore shape and degree of pore uniformity. Gas sorption isotherm curves were analyzed by BJH and and BET calculations to obtain pore size distributions, surface area, and pore volumes.

3.6.1 Volume Shrinkage

Sample measurements were taken in order to quantify the changes in sample shapes occurring during the drying and sintering stages of processing. The initial cylindrical volume of each sample was known as all samples were poured to fill the same circular dish mold with a diameter of 7 cm and a height

of 1.25 cm. Calipers were used to take rough measurements of the height and diameter of each green body after the drying step was completed. These measurements were also repeated after sample firing. Percent volume shrinkage occurring during drying, firing, and total volume shrinkage were calculated and compared between sample types.

3.6.2 Archimedes Porosity Measurements

Archimedes' principle provides a relatively quick and simple way to obtain porosity measurements (open, closed, and total) of fired samples. Samples were weighed dry in air (W_{dry}), submerged in water and weighed in air again (W_{water}), and weighed while suspended in water using a spring scale ($W_{suspended}$). The amount of open porosity (porosity within the sample that is open to the air) can be obtained by subtracting the weight of the dry sample from the weight of the sample filled with water. The difference between these two values, taken with the density of water (ρ_{water} = 1.00 g/cc) provides the volume of water that fills the open pores in the sample. The calculation for volume of open pores (V_{open}) is related by Equation 2.

$$V_{open} = \left(W_{water} - W_{dry} \right) * \rho_{water} = \left(W_{water} - W_{dry} \right) \qquad \text{Eq. 2}$$

The amount of closed porosity can be determined by taking into account Archimedes' principle, which states that the buoyant force of an object suspended in water is equal to the weight of water that the object displaces. Because the open pores of the sample were not covered when the samples were suspended in water, the water displaced is equal to the volume of ceramic and the volume of closed pores only. Equation 3 for the volume of closed pores (V_{closed}) is derived below.

$$W_{sus} = W_{dry} - W_{displaced\ water}$$

$$W_{sus} = W_{dry} - (V_{ceramic} + V_{closed})$$

$$V_{closed} = W_{dry} - W_{suspended} - V_{ceramic}$$

$$V_{closed} = W_{dry} - W_{suspended} - \frac{W_{dry}}{\rho_{ceramic}} \quad \text{Eq. 3}$$

The values of V_{open}, V_{closed}, and the theoretical density of alumina (3.97 g/cc) were used to calculate the total amount of porosity in the samples. The bulk volume (volume of open pores, volume of closed pores, and volume of ceramic component) was calculated for each sample and used to calculate the percent of open, closed, and total porosities in each sample. Comparisons between porosity measurements were made using a t-test at the 95% confidence interval. Two porosity values were considered statistically different if the values within their 95% confidence intervals did not overlap. The equation for the 95% confidence range is related by Equation 4.

$$95\%\ CI = \bar{X} \pm\ t * \frac{s}{\sqrt{n}} \quad \text{Eq. 4}$$

Here, $\bar{X}$ is the sample mean, t is the t-statistic based on the number of samples tested, s is the standard deviation for all samples, and n is the number of samples. Because the sample size was always equal to 3, the two-tailed t-statistic for a 95% confidence interval was 4.303.

3.6.3 Optical Microscopy

Optical images were obtained using an Olympus SZH10 research stereo microscope. Varying magnification levels were used to observe samples. Images were taken of the spherical ice particles, both small and large, prepared for this study. Because the ice particles tended to melt very quickly under the microscope light, images had to be taken very quickly. Optical micrographs were also obtained for the final porous alumina structures after being fired. These images were intended to provide a general idea of the structure of different porous alumina samples. Qualitative assessment on pore size, shape, and uniformity can be made with these images.

3.6.4 Scanning Electron Microscopy

Samples were cut to an appropriate size using a diamond saw and were then mounted onto a sample holder and coated around the edges with silver paint for SEM (Scanning Electron Microscope) imaging. Images were acquired at the Virginia Tech Institute of Critical Technology and Applied Science Nanoscale Characterization and Fabrication Laboratory (VT ICTAS NCFL) with a LEO (Zeiss) 1550 field-emission SEM (Figure 9). A working distance of 6-8mm and EHT of 5.00 kV was used. Varying magnification levels were used to observe samples.

Figure 9 Leo Zeiss 1550 FESEM

3.6.5 Gas Sorption

Gas sorption was performed using a Quantachrome Autosorb-1 system. Four different samples were tested. Samples were placed in a 9mm tube with a rod and outgassed at 300˚C for approximately 24 hours. Nitrogen was used as the absorbate gas and analysis was performed measuring 10 adsorption and 10 desorption points. The Quantachrome data analysis software produced a linear isotherm plot for each sample tested. The general shape of sorption isotherm curves can provide information about the porosity of the studied sample. Isotherm shapes are typically classified into one of six types, each type revealing information on the ability of the adsorbate to interact with the adsorbent and the relative size of pores within the structure [58]. The six isotherm shapes, classified by the International Union of Pure and Applied Chemistry (IUPAC), are shown in Figure 10 [59].

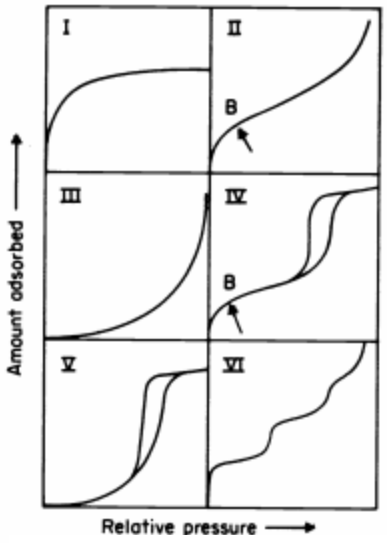

Figure 10 IUPAC classifications of sorption isotherms [59]

The Barrett-Joyner-Halenda (BJH) method was used on the isotherm desorption curve to obtain a plot of cumulative pore volume as a function of pore radius. The nature of the desorption process is typically more stable than adsorption [58] and so the desorption isotherm curve was used to obtain pore size distributions. The BJH method also provides information regarding the surface area and total pore volume of each sample.

The four samples analyzed by gas sorption methods are summarized below in Table 6. These samples were specifically selected to look at the effect of changes in amount of ice added and freezing method on the pore size distribution. The presence of pores within the control sample (which didn't use any ice) was also of high interest.

Table 6 Samples analyzed by gas sorption

Sample Number	System	Ice	Setting Method	Sintering Temperature
A C.1	Alumina	0 vol%	Freezer	1500
A 2.4	Alumina	43 vol% small spherical	Freezer	1500
A 2.5	Alumina	43 vol% small spherical	Liquid Nitrogen	1500
A 4.1	Alumina	75 vol% small spherical	Freezer	1500

Chapter 4. Results

Chapter 4 summarizes the results obtained from the experimental procedure outlined in Chapter 3. These results are further analyzed and discussed in context of the entire process in Chapter 5.

4.1 Volume Shrinkage

Sample dimensions were measured after the drying process and after sintering. Figure 11 shows a green body after firing. Large cracks have developed throughout the part. Figure 12 depicts the amount of shrinkage resulting from drying for samples with and without agarose. The presence of agarose does not appear to alter the amount of shrinkage experienced during drying. Shrinkage sharply increases as more ice is added to the slurry. A large increase in shrinkage is seen at 56 vol% ice addition. Most samples were quite brittle after the drying process, but remained intact in their cylindrical shape and could still be handled. This was not the case for samples which used 75 vol% ice, which essentially fell apart after drying. Samples which had 75 vol% were extremely thin and fragile. Volume measurements were taken of the collapsed dried green bodies, however it was very difficult to collect pieces to be placed in the furnace for sintering. In fact, the alumina/ agarose sample which contained 75 vol% ice could not be handled at all and was not able to be sintered.

Figure 11 Dried green body subjected to cracking and volume shrinkage

Figure 13 illustrates the volume shrinkage after sintering as a function of sintering temperature used. Sintering temperatures appear to linearly affect the amount of volume shrinkage, as seen by the trend line superimposed on the graph. Samples shrank equally in all dimensions during the solid-state sintering process.

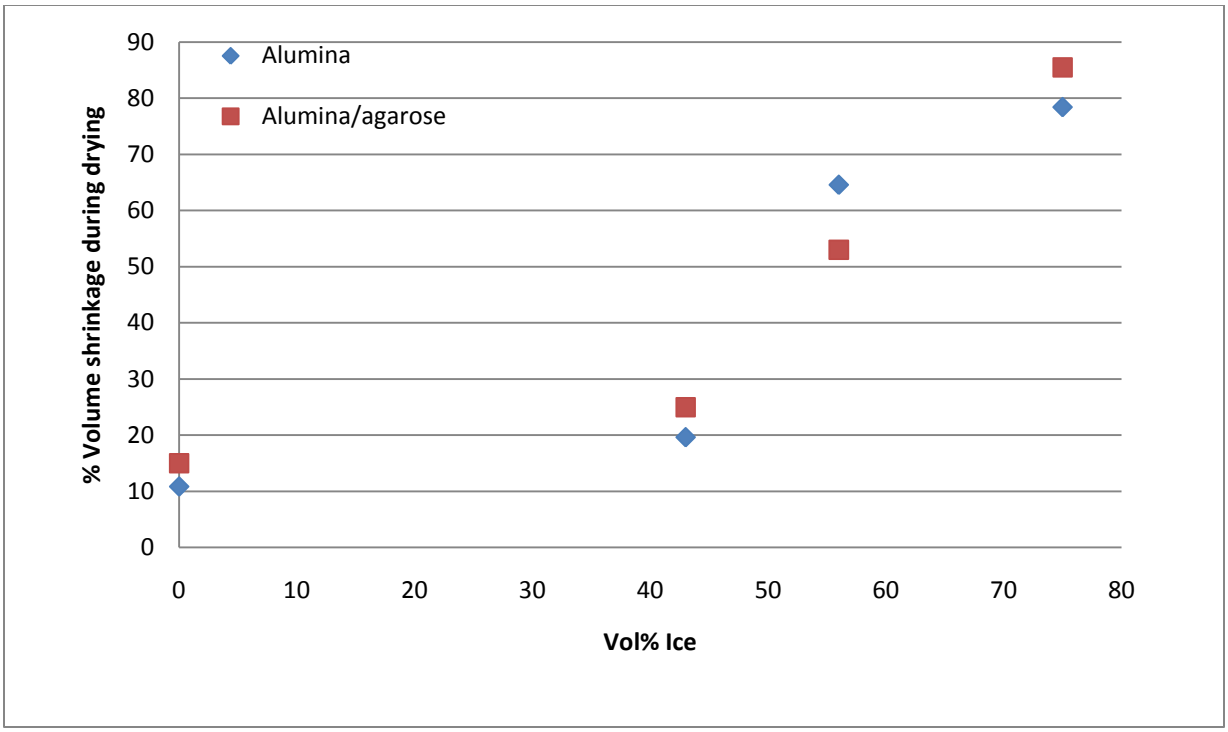

Figure 12 Volume shrinkage during drying as a function of vol% ice added to slurry, samples fired at 1500˚C

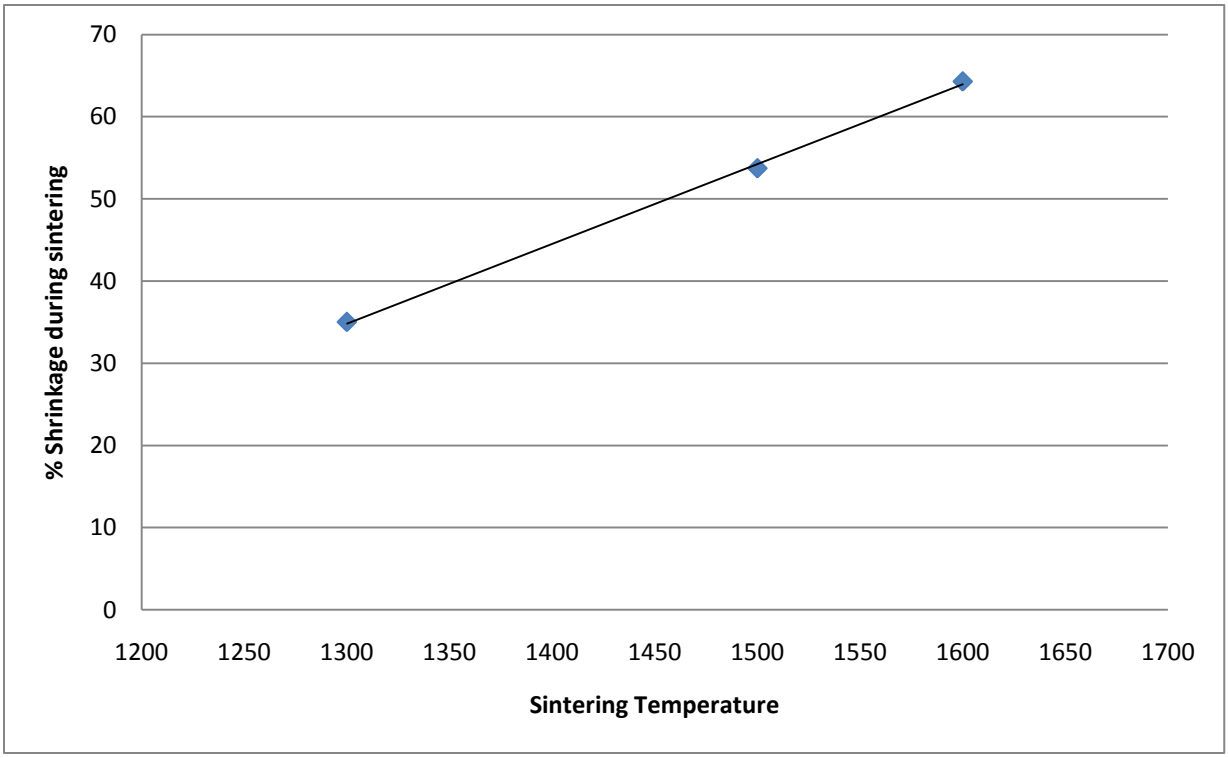

Figure 13 Volume shrinkage during sintering as a function of sintering temperature, 43 vol% ice used

4.2 Archimedes Porosity Measurements

Archimedes Principle was used to estimate the amount of open, closed and total percent porosities within samples as described in Chapter 3. This analysis allows for identification of the type of porosity that is present (open or closed) and it can also reveal shifts in porosity type and amount during processing.

4.2.1 Porosity vs. Volume % Ice Added to Slurry

Figure 14 illustrates the changes in porosities (total, open and closed) versus the volume percent of ice that was added to the alumina slurry. Each of the samples presented in this figure underwent the exact same set of processing steps except for the amount of ice introduced to the slurry. Samples were made without agarose gelling agent, used small spherical ice particles, were frozen in a freezer, and were subsequently sintered at 1500˚C after drying. Each data point represents the average porosity measured from three different samples and the error bar spans two sigma of the sample population.

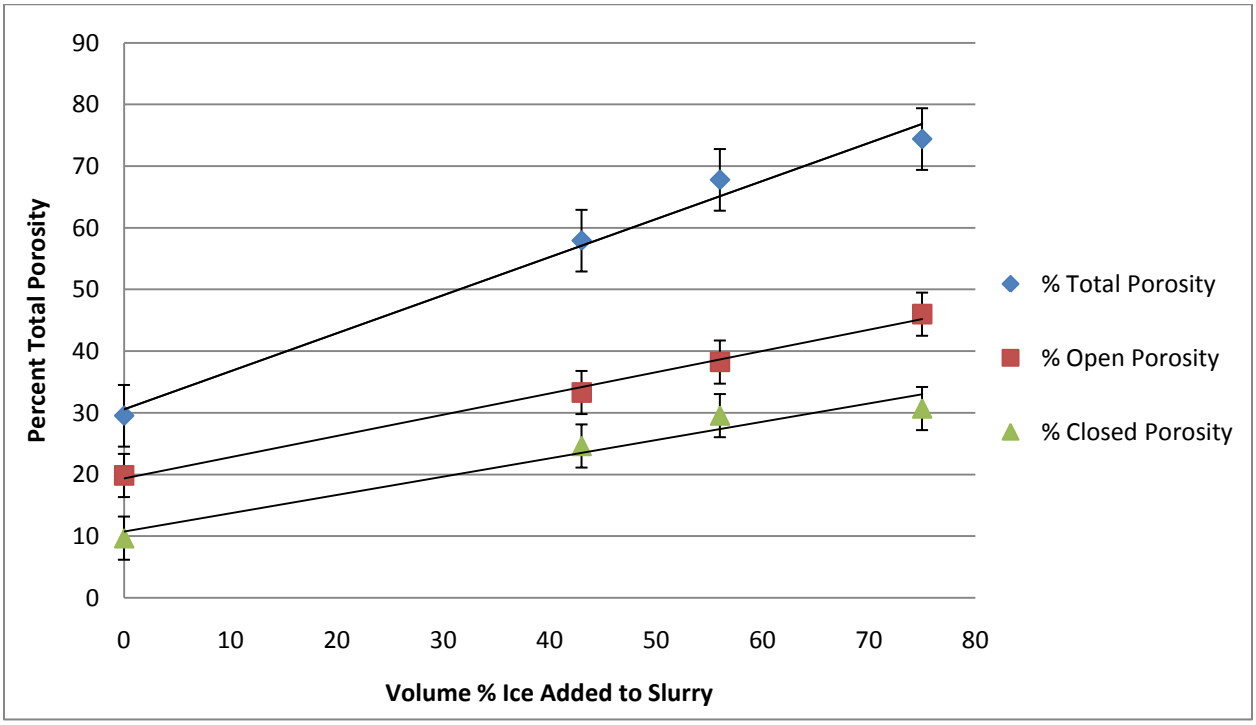

Figure 14 Percent porosity as a function of volume percent ice added to the slurry for alumina samples fired at 1500˚C

A large increase in porosity from 0 vol % ice to 43 vol% ice is evident. Samples with 43 vol% ice had almost double the porosity of samples which contained no ice. For the data points included in this figure, the correlation appears to fit a linear curve. The t-test was utilized at a 95% confidence interval to determine the statistical significance of changes in porosity between 43, 56, and 75 vol% ice. At 95% confidence, the samples with 75 vol% ice had a significantly higher porosity than samples with 43 vol% ice. Samples with 56 vol% ice however, were significantly different from the samples with either 43 or 75 vol% ice at an 85% confidence. Samples that were prepared without any ice had open as well as closed porosity in the final fired samples.

Percent open and closed porosities steadily increase as more ice is added to the slurries. The differences observed in closed porosity for the three samples with ice are not statistically significant when compared using the t-test. The open porosity present in the same with 75 vol% ice is significantly higher from the open porosity seen in the sample with 43 vol% ice.

Figure 15 depicts the changes in porosities (total, open, and closed) as a function of the volume percent of ice that was added to the alumina agarose samples.

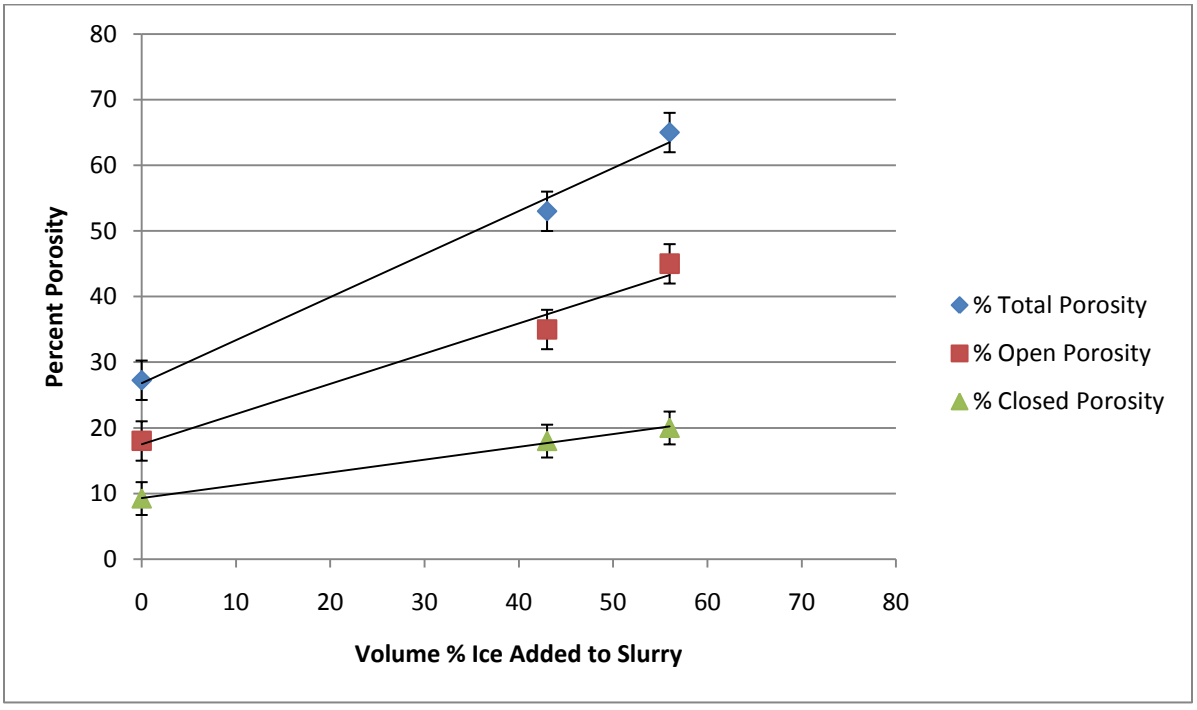

Figure 15 Percent porosity as a function of volume percent ice added to the slurry for alumina/agarose samples, fired at 1500˚C

Each of the samples presented here were subjected to the same processing conditions except for the amount of ice introduced to the slurry. Samples were made of the alumina/agarose system, used small spherical ice particles, were set and dried on a lab bench, and were fired at 1500˚C. It should be noted that data does not exist for samples with 75vol% ice. These samples completely collapsed during the drying stage and porosity measurements could not be taken.

The porosity values presented in this figure are comparable to porosity values seen in samples without agarose in Figure 14. An overall increase in porosity is observed as more ice is added to the slurry. The amount of closed porosity does not significantly change from 43 to 56 vol% ice, however, a significant increase is observed in the % open porosity.

4.2.2 Porosity vs. Sintering Temperature

Figures 16 and 17 depict the percent porosities (open, closed, and total) resulting from samples sintered at all three sintering temperatures. The ice used for the samples in Figure 16 was blended ice and small spherical ice particles were used to make the samples seen in Figure 17. These samples were made of alumina only systems, used 43 vol% ice, and were frozen in a freezer.

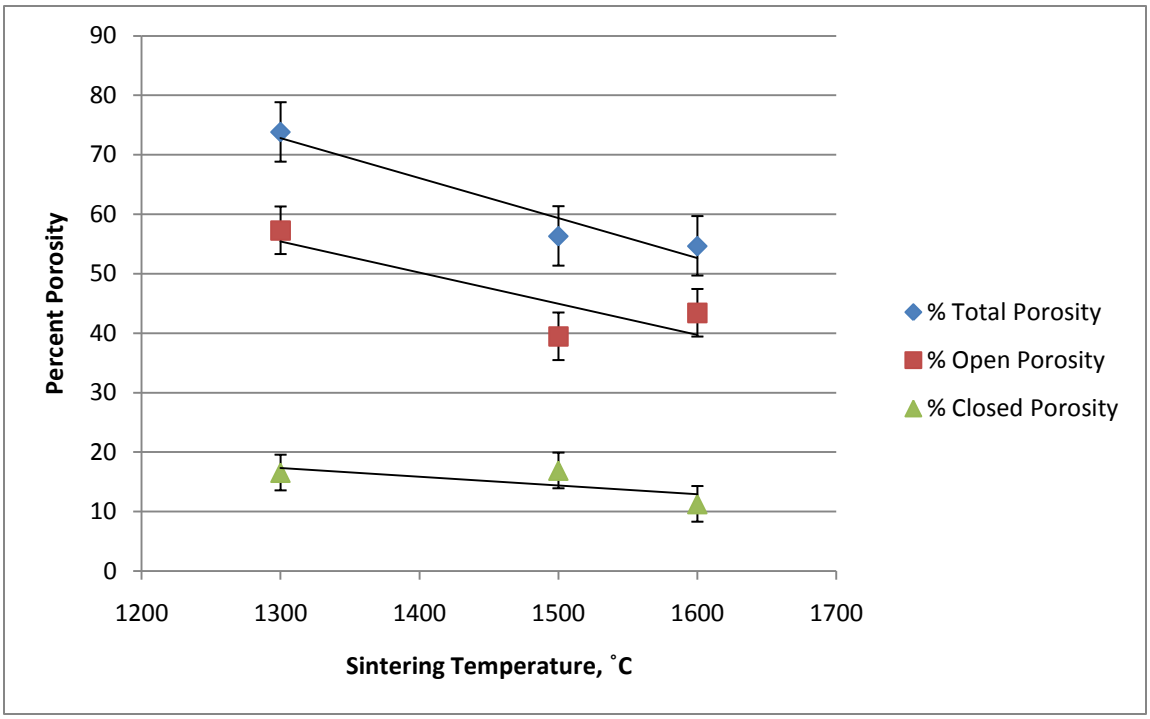

Figure 16 Percent porosity versus sintering temperature with 43 vol% blended ice

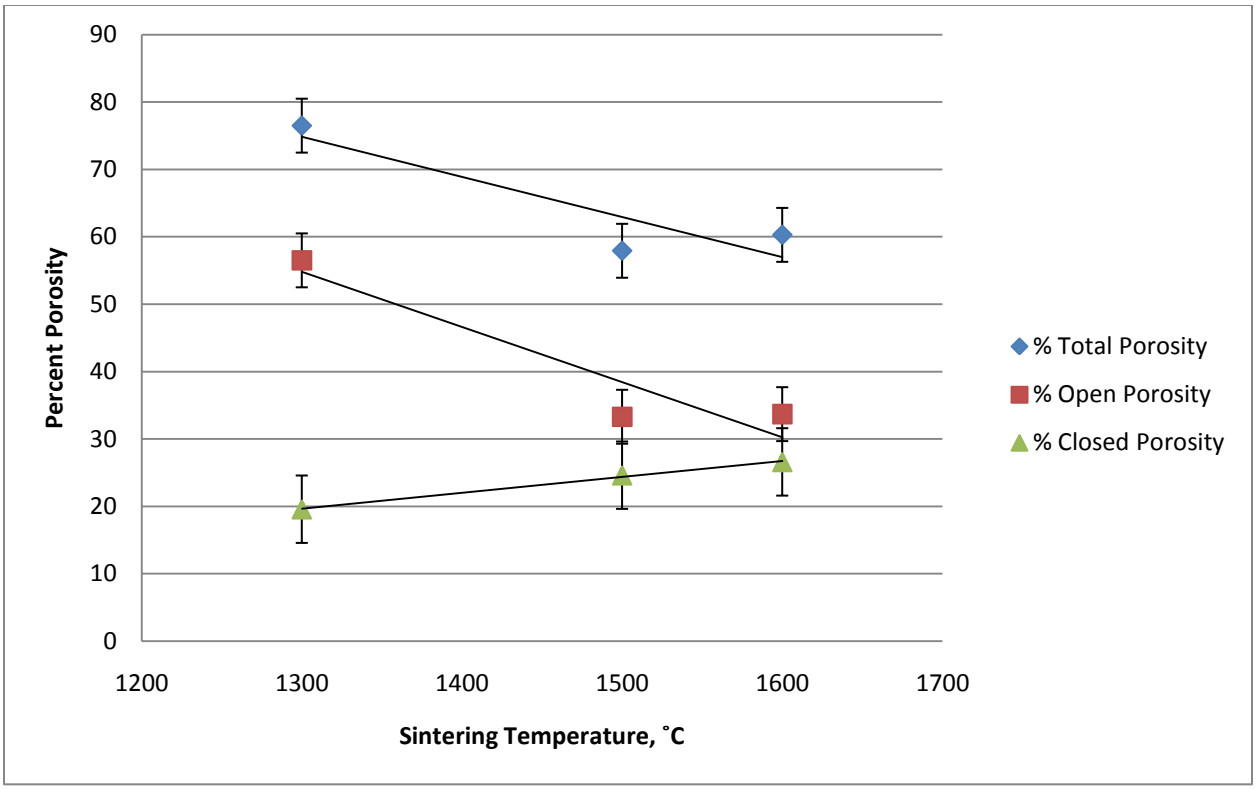

Figure 17 Percent porosity versus sintering temperature with 43 vol% small spherical ice

Both figures indicate a significant decrease in total porosity from 1300˚C to 1500˚C. No significant changes were observed in any of the porosity types when the sintering temperature was increased from 1500˚C to 1600˚C. Both sets of samples indicate a significant decrease in open porosity when sintering temperature is increased from 1300˚C to 1500˚C. Closed porosity does not appear to be affected by sintering temperature in either set of samples. It is also noted that the % total porosity values are comparable between the samples prepared with blended ice and samples prepared with small spherical ice. Samples prepared with small spherical ice tended to have a higher amount of closed porosity (especially at higher sintering temperatures) than the samples prepared with blended ice.

Figure 18 shows the percent porosities (open, closed, and total) present in alumina samples that were frozen in liquid nitrogen and sintered at all three temperatures. The slurries used to prepare these samples contained 43 vol% small spherical ice particles.

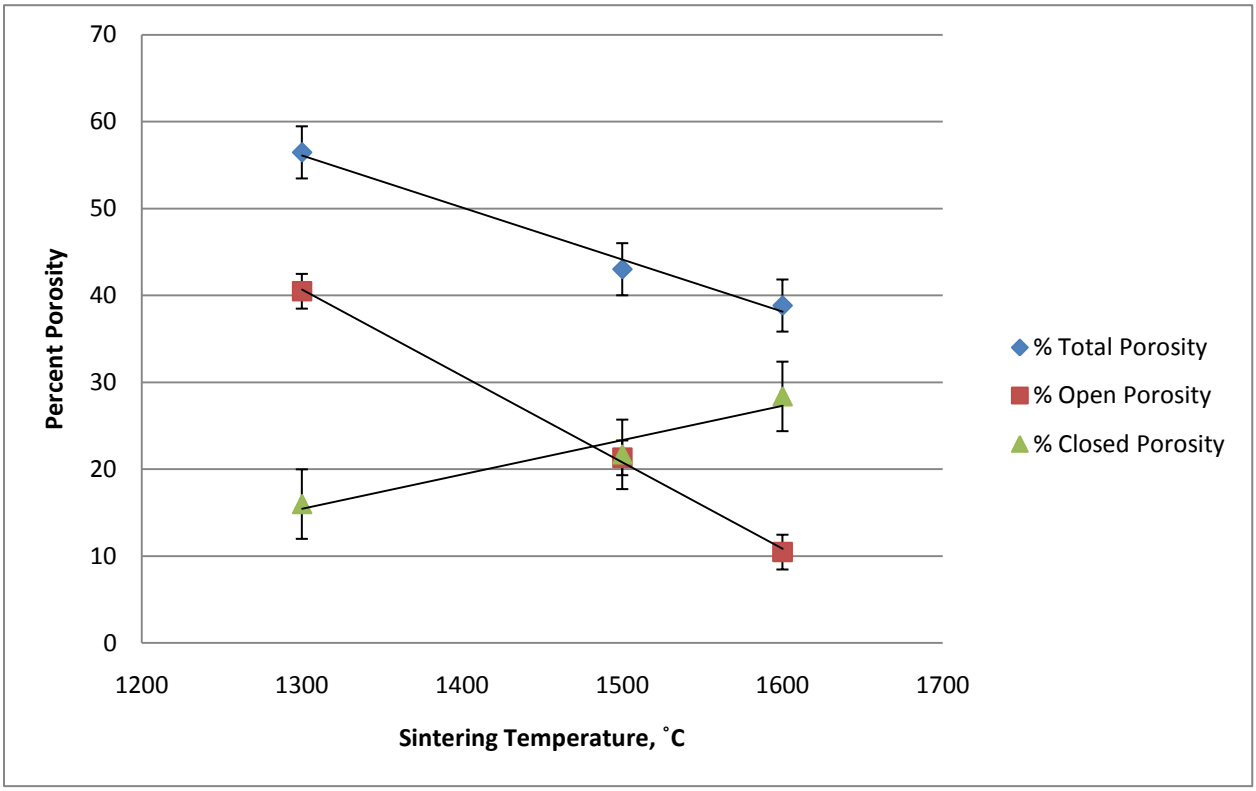

Figure 18 Percent porosity versus sintering temperature when frozen in liquid nitrogen, prepared with 43 vol% small spherical ice

Similar to the two previous figures, increasing sintering temperature causes a decrease in the total amount of porosity observed in samples; however, these samples have significantly lower porosity levels than samples that were frozen more slowly in a freezer. Samples frozen in liquid nitrogen also see a sharper increase in the amount of closed porosity and a sharper decrease in the amount of open porosity as higher sintering temperatures are used.

4.3 Optical Imaging

4.3.1 Ice Particle Imaging

Figure 19 depicts the large spherical ice particles used in this experiment. Images had to be taken quickly before the ice particles began to melt. These ice particles averaged approximately 3 mm in diameter and all particles exhibited relatively decent uniformity in size and spherical shape as can be seen in the figure below.

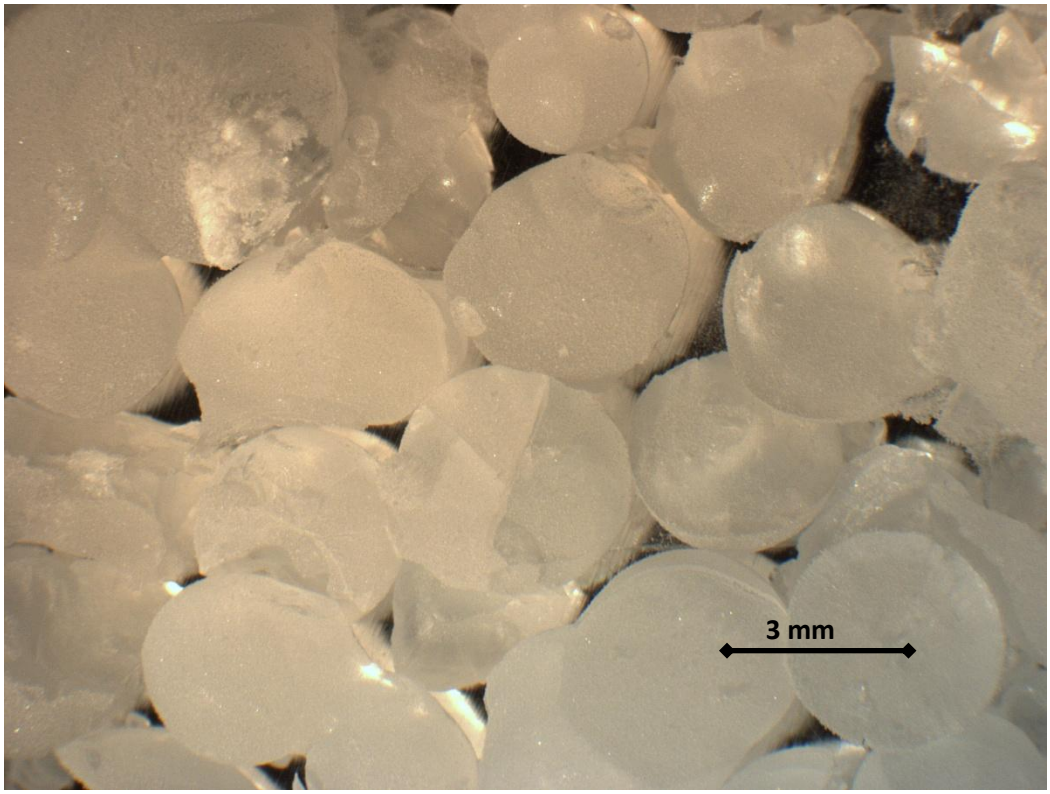

Figure 19 Large spherical ice particles

Figure 20 depicts the optical image taken of the small spherical ice particles used in this study. These images were significantly more difficult to capture because the small ice particles would rapidly melt when placed under the microscope. The image presented is the best image that could be obtained where the ice particles can be seen. Particle size diameters typically ranged anywhere between 100 and 200 microns. The average particle diameter was about 150 microns in diameter.

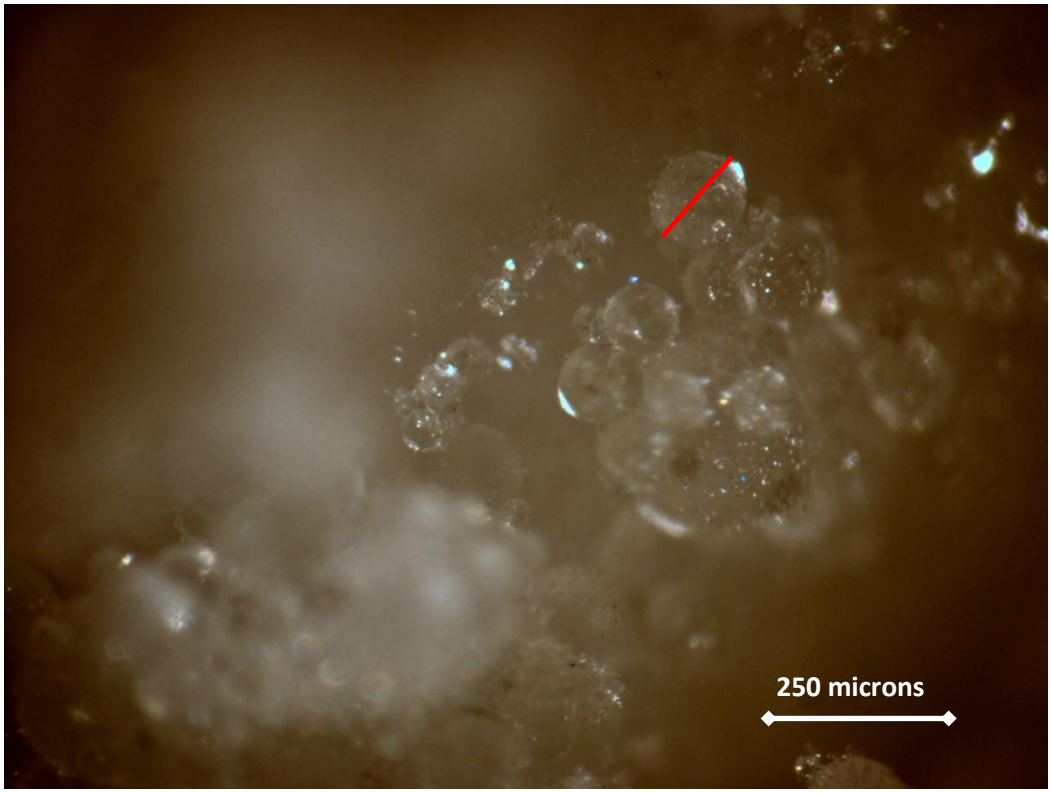

Figure 20 Small spherical ice particles

4.3.2 Porous Alumina Imaging

Figures 21-25 are presented below to give an idea of what the final porous alumina parts looked like. Qualitative assessments were made on pore shape, size, uniformity, and distribution with these images. Clear differences are observed in the sizes of pores resulting from the large and small spherical ice particles. Figure 21 depicts a sample made from large ice particles. It has large pores ranging anywhere from 0.5 to 2 mm. Figure 22 shows a sample made from the smaller ice particles. These are significantly smaller in size ranging from a few tens of microns up to 200 microns. The pores observed in both of these figures are relatively round in shape and evenly dispersed throughout the sample. Figure 23 is an optical micrograph of a control sample which was made without using any ice. While the surface of the sample is somewhat rough, no pores are visible. Figures 24 and 25 show one pore in a sample made with 43 vol% blended ice. Using different focusing settings, interconnected porosity is observed further inside of the sample.

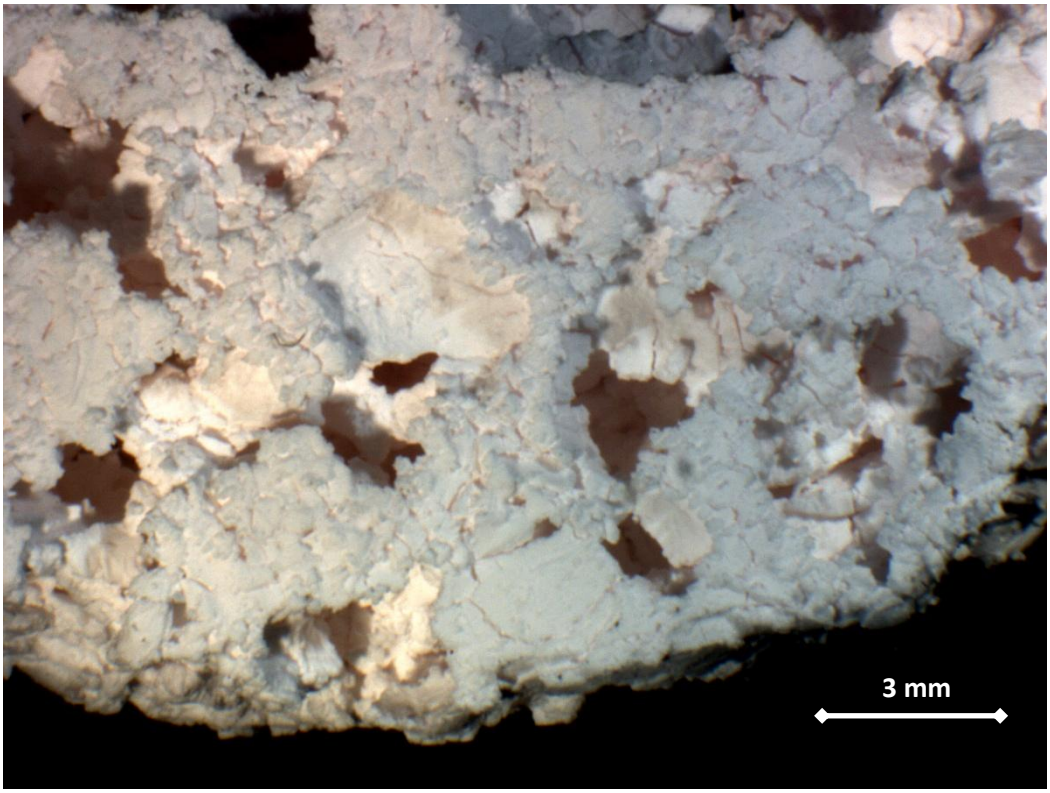

Figure 21 Pores resulting from large spherical ice particles, fired at 1500˚C

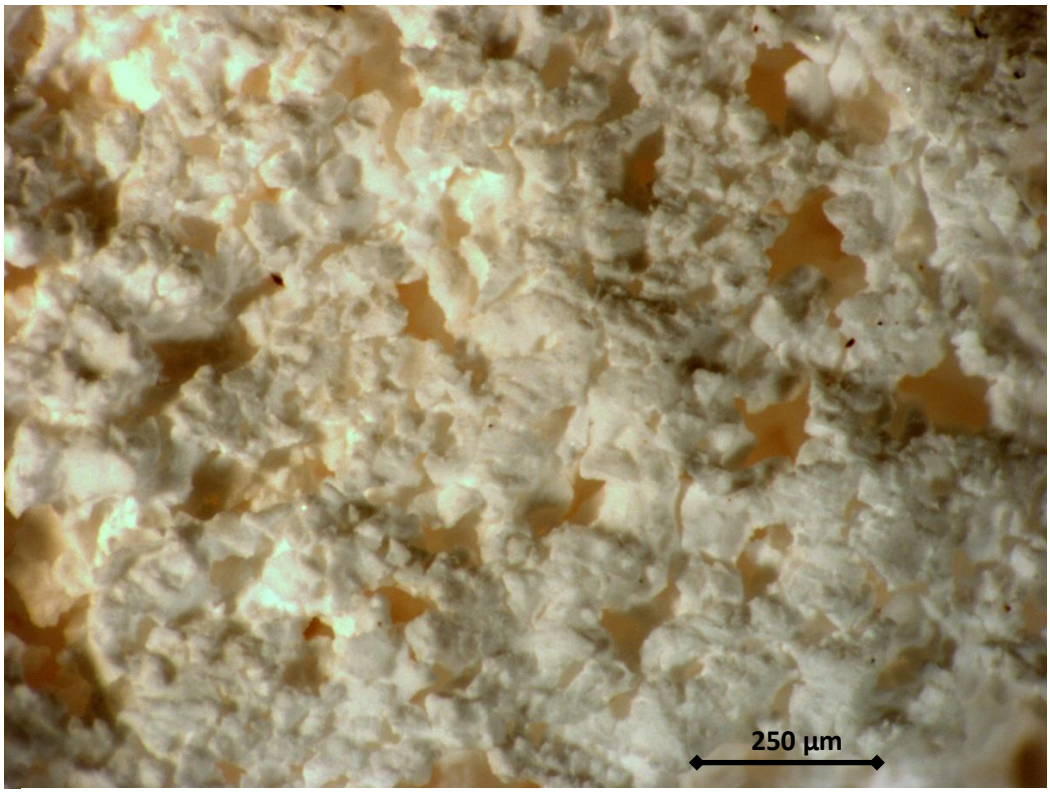

Figure 22 Pores resulting from small spherical ice particles, fired at 1500˚C

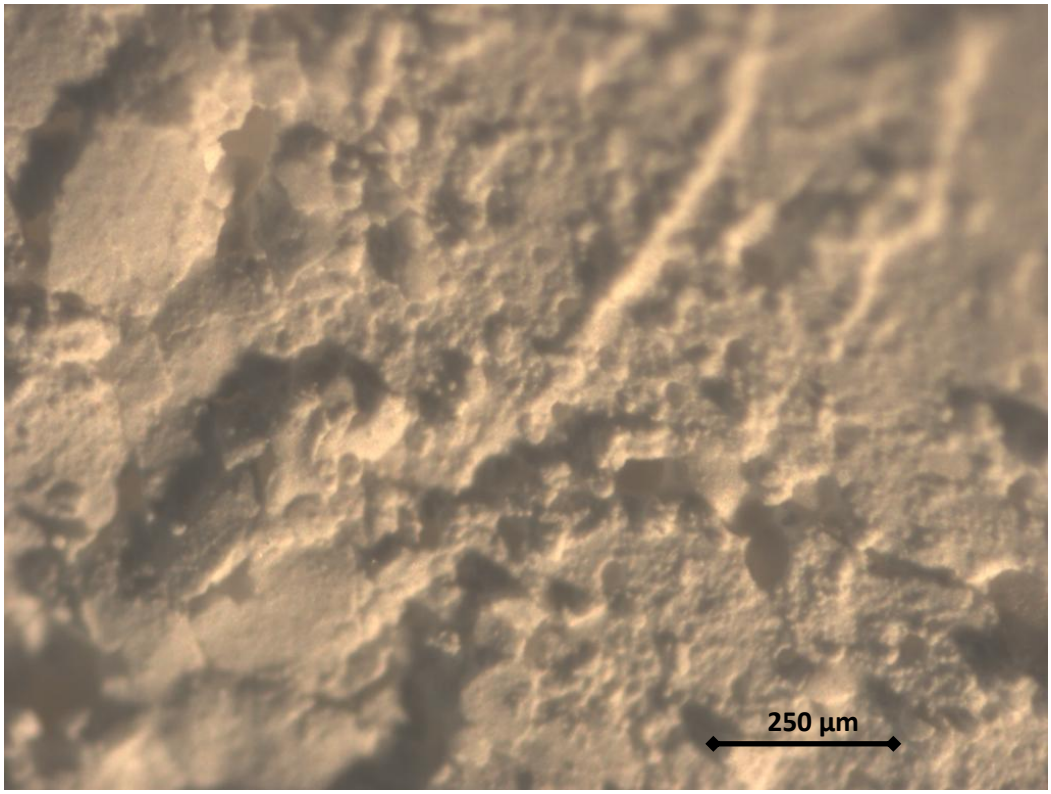

Figure 23 No pores observed in control sample without ice, fired at 1500˚C

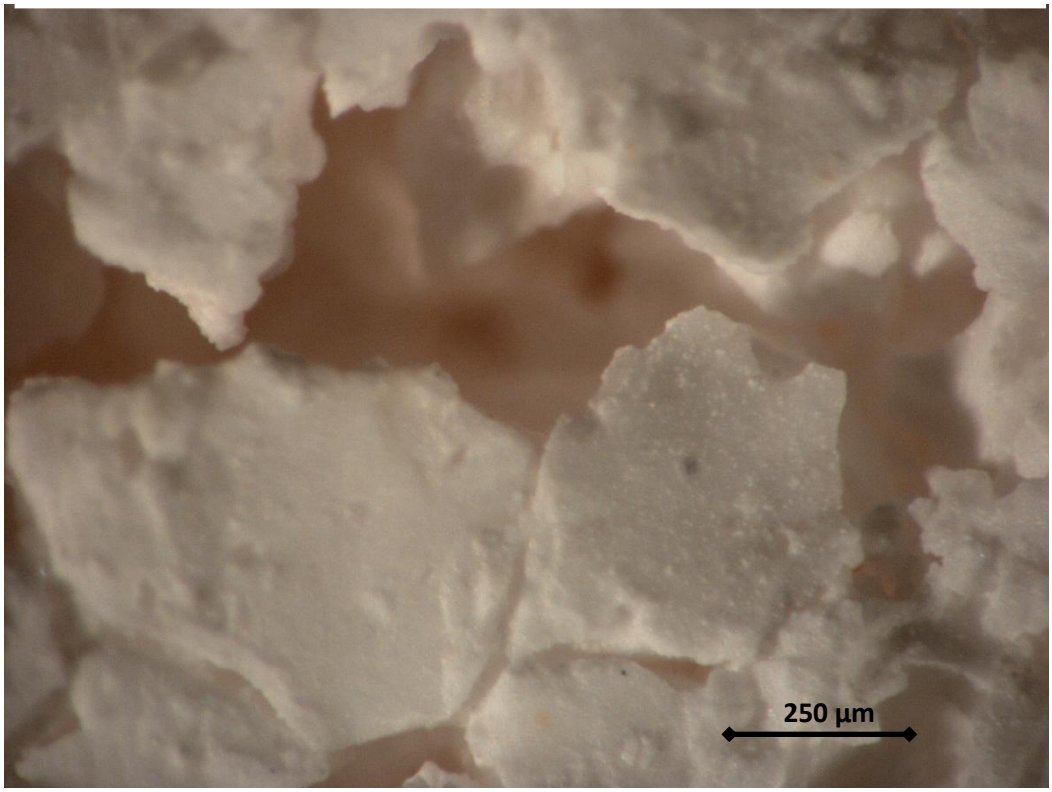

Figure 24 Open pore leading to interconnected porosity

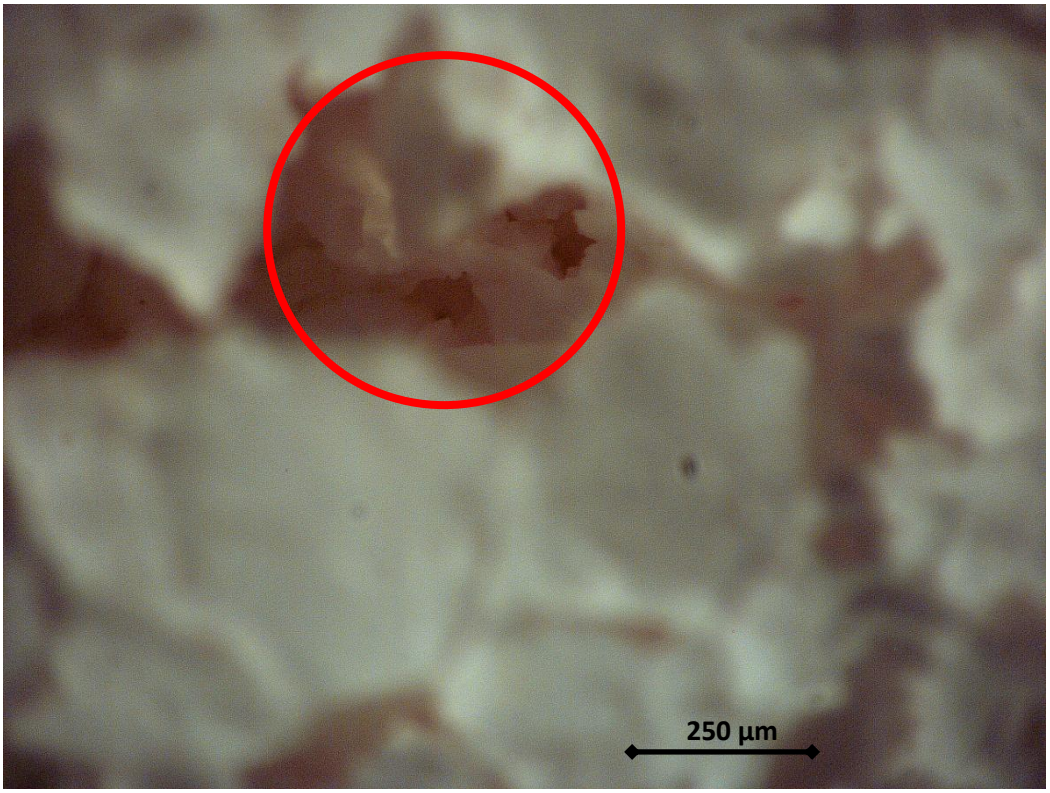

Figure 25 Presence of interconnected porosity

4.4 Scanning Electron Microscopy

SEM images were obtained and analyzed to observe differences in samples resulting from changes in the vol% ice added, size and shape of ice added, freezing method, sintering temperature used and the presence of agarose gelling agent. Figure 26 at a magnification of 10,290x and Figure 27 at a magnification of 9,810x depict the typical microstructures observed for samples sintered at either 1300 or 1500˚C.

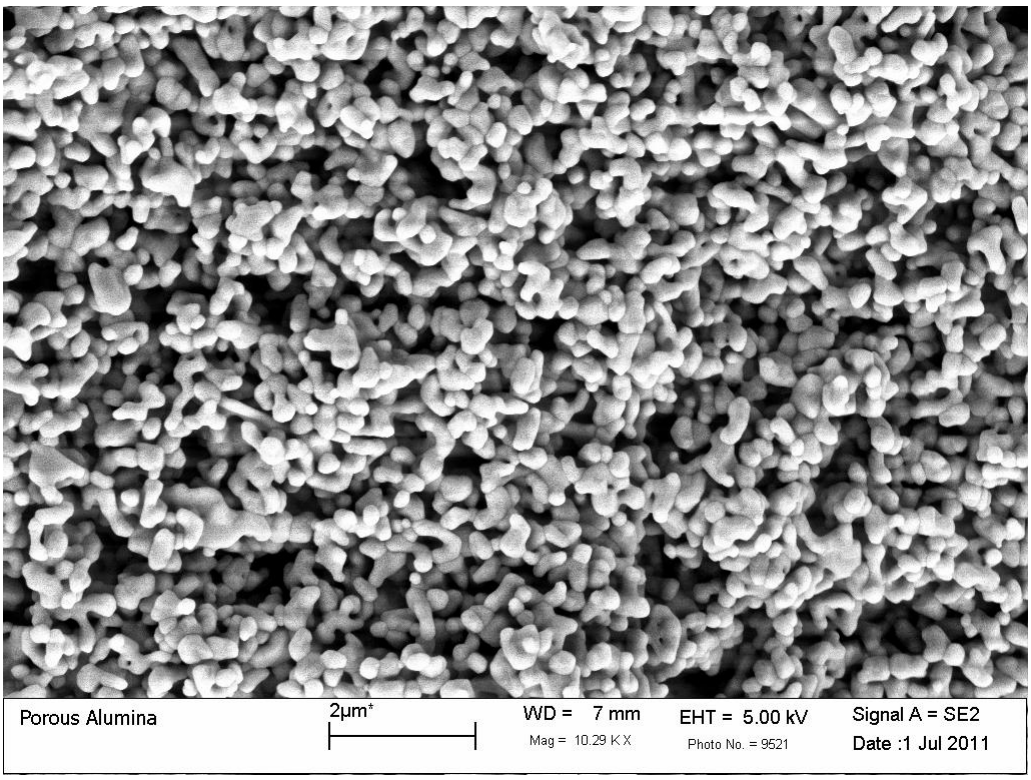

Figure 26 Typical microstructure of a sample sintered at 1300˚C

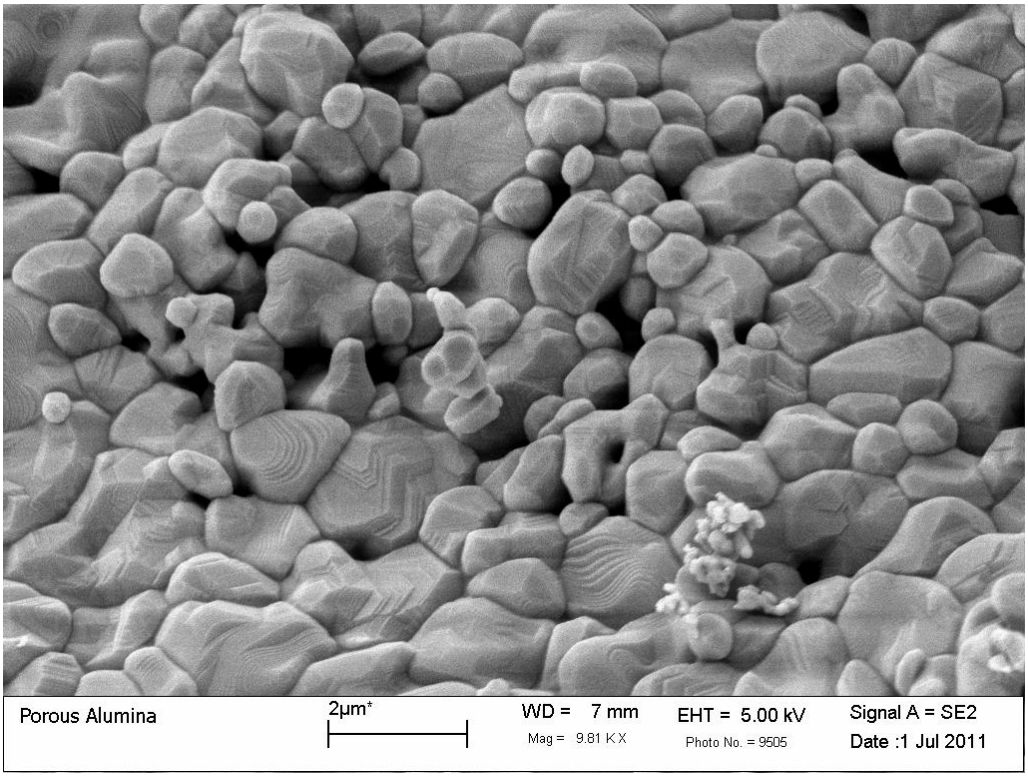

Figure 27 Typical microstructure of a sample sintered at 1500˚C

A large majority of the ceramic particles seen in Figure 26 are 0.25μm with a few being slightly larger around 0.4μm. The particles are still quite spherical in shape. High amounts of porosity are visible throughout the sample with an extensive amount of interconnectivity. The ceramic particles seen in Figure 27 are significantly larger. Particle sizes range anywhere from 0.25μm to 2μm, with the majority of particles at the larger end around 2μm. Porosity has significantly decreased and pores do not appear to be interconnected to one another. These closed pores are around 0.25-0.5μm in size.

Figures 28 and 29 depict the sample made with 43 vol% ice and sintered at 1500˚C. Two different magnifications are used. Pores in these samples range in size from approximately 20μm to 200μm. Most of the pores are relatively round in shape, although a few of the very large pores seen in Figure 28 are more oval in shape. The pores presented in Figure 29 are quite uniform in size and shape. They are approximately 20 μm in size.

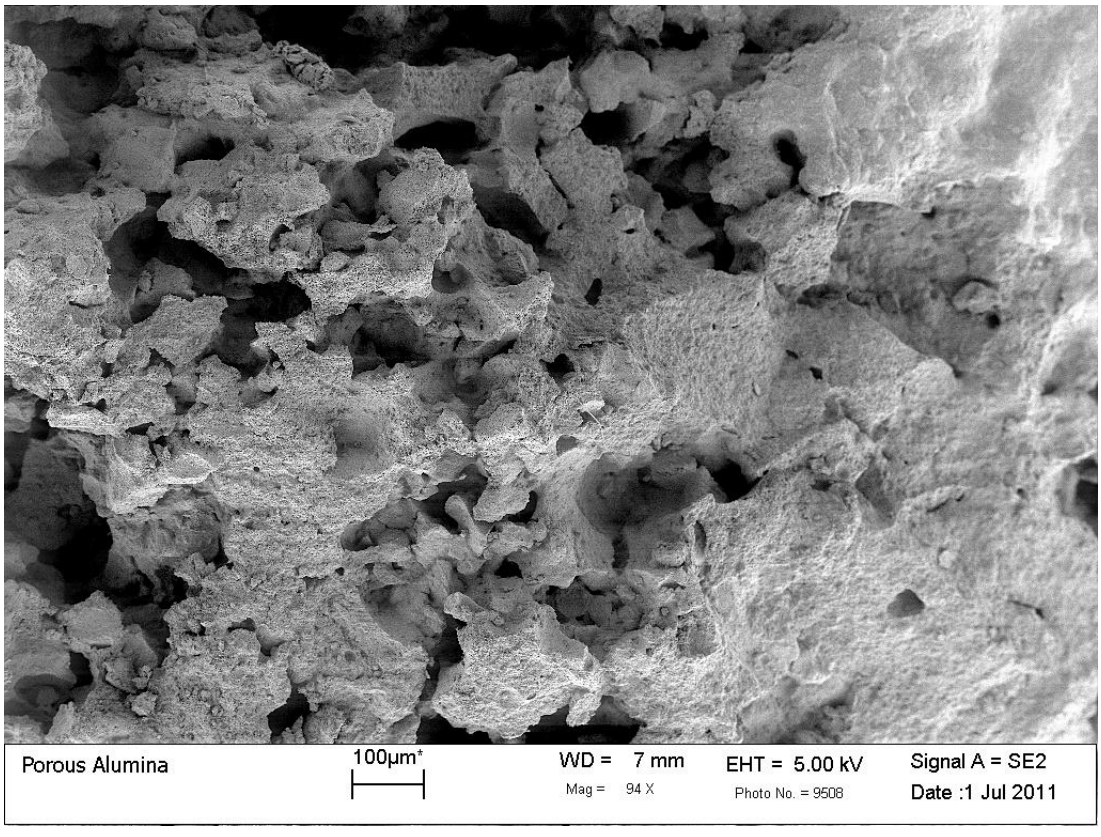

Figure 28 Porosity in sample with 43 vol% small spherical ice, fired at 1500˚C

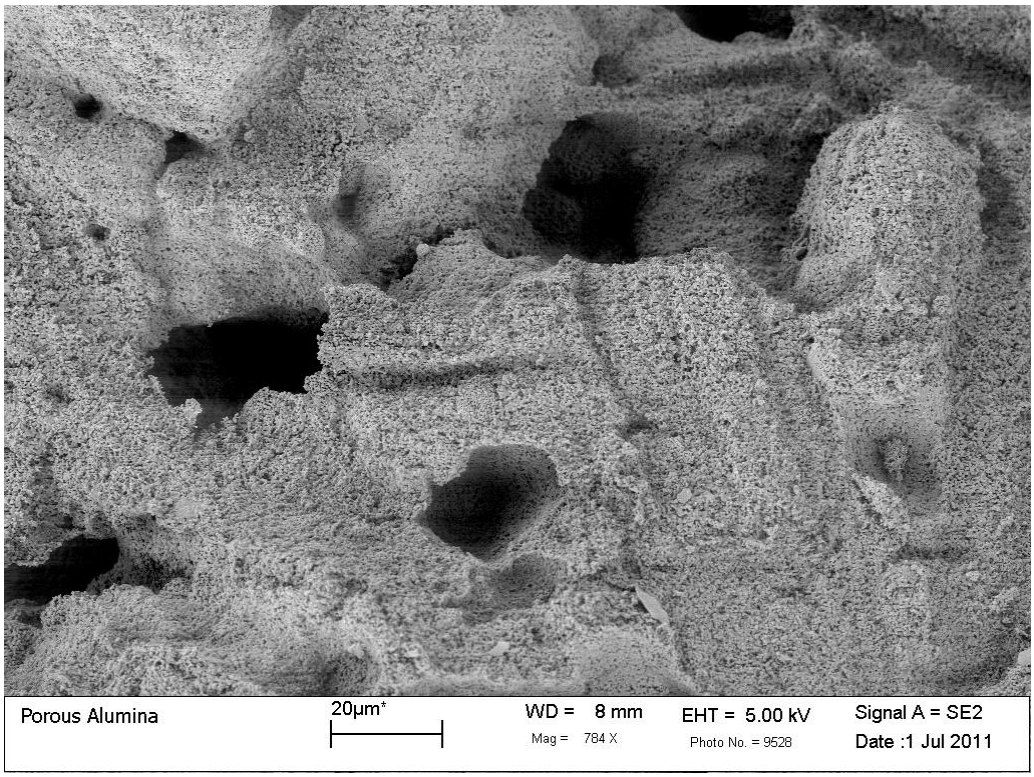

Figure 29 Close-up of pores in sample with 43 vol% small spherical ice, fired at 1500˚C

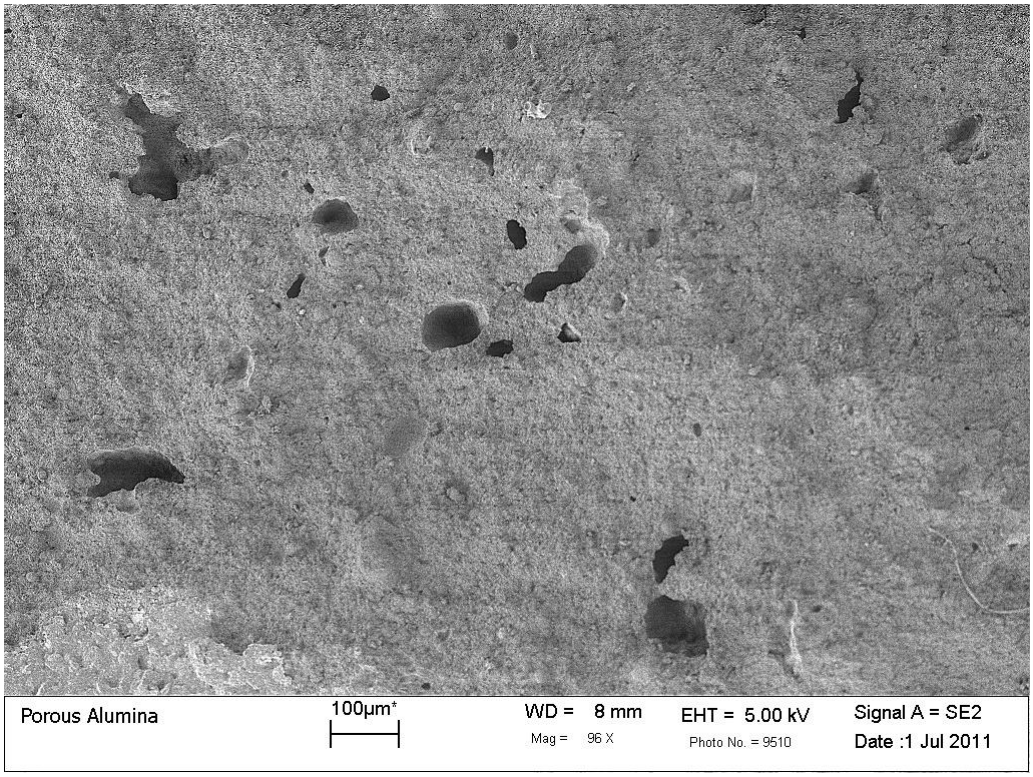

Figure 30 Porosity in sample frozen in liquid nitrogen, fired at 1500˚C

Figure 30 shows the surface of the samples prepared with 43 vol% small spherical ice and frozen quickly in liquid nitrogen. The pores in this sample are sparsely distributed throughout the sample and do not appear to be interconnected to one another. Pores range in size from about 20μm to 100μm. Figure 31 depicts the pore structure of the control alumina sample which did not contain any ice. Pores on the order of 10μm are not visible in this image.

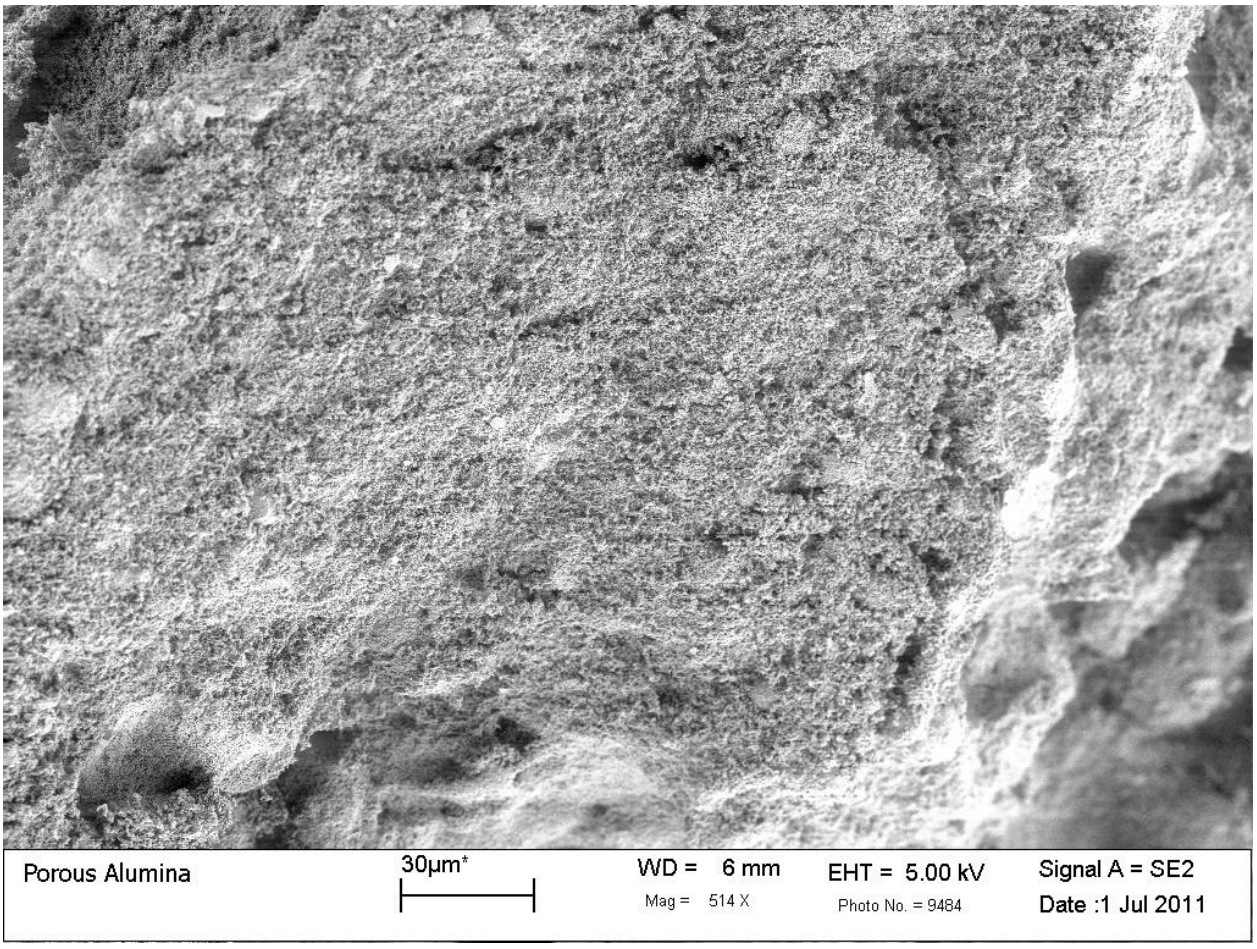

Figure 31 Porous structure of control sample prepared without ice, fired at 1500˚C

Figure 32 presents the microstructure observed in the alumina/agarose sample prepared with 43 vol% ice. Pores are visible, ranging from about 50 to 200μm.

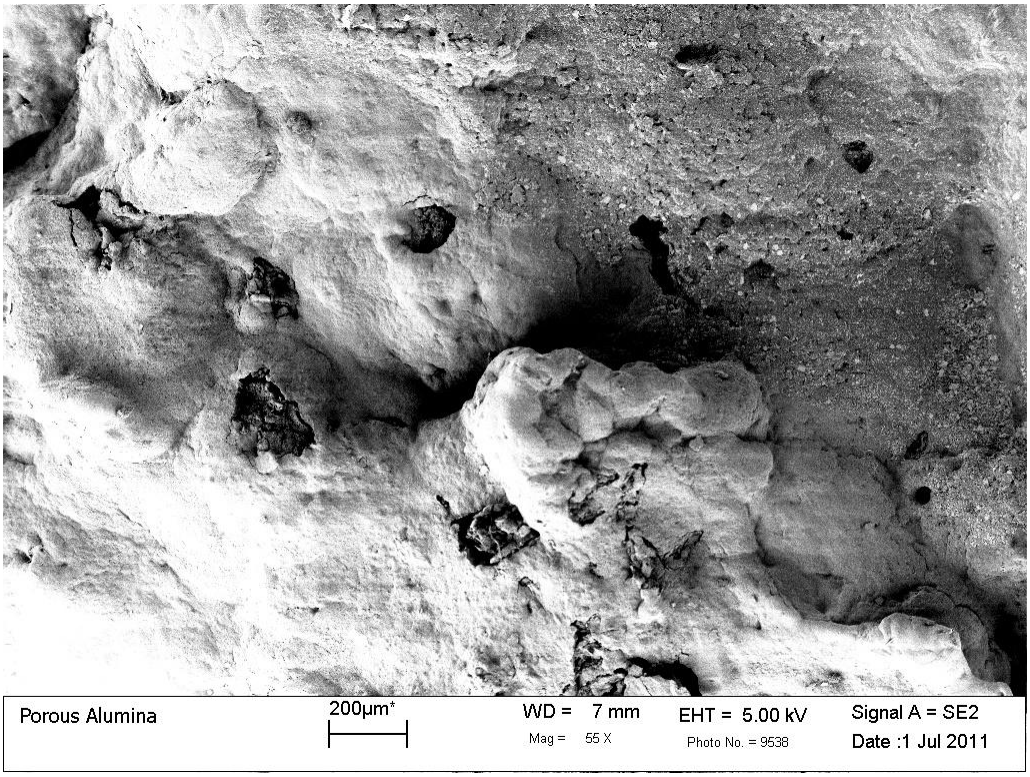

Figure 32 Porosity within alumina/agarose sample, fired at 1500˚C

4.5 Gas Sorption

4.5.1 Isotherm Curves

Pore size distributions were obtained using gas sorption methods. Figures 33-36 depict the linear isotherm plots obtained from four samples characterized by gas sorption. The red line represents the adsorption curve and the desorption curve is shown in blue. All samples tested in gas sorption were made purely of alumina and were fired at a temperature of 1500˚C. Figure 33 represents the sorption isotherm for a control sample prepared without ice. The isotherm seen in Figure 34 was generated from a sample prepared with 43 vol% small spherical ice and frozen in a freezer. Figure 35 represents a sample that was quickly frozen in liquid nitrogen, and Figure 37 represents a sample prepared with 75 vol% small spherical ice. All plots show an isotherm curve with the same relative shape. The isotherm curves in Figures 33-35 are characterized by a slight hysteresis loop at the higher end of P/P_0. Figure 36 has no visible hysteresis.

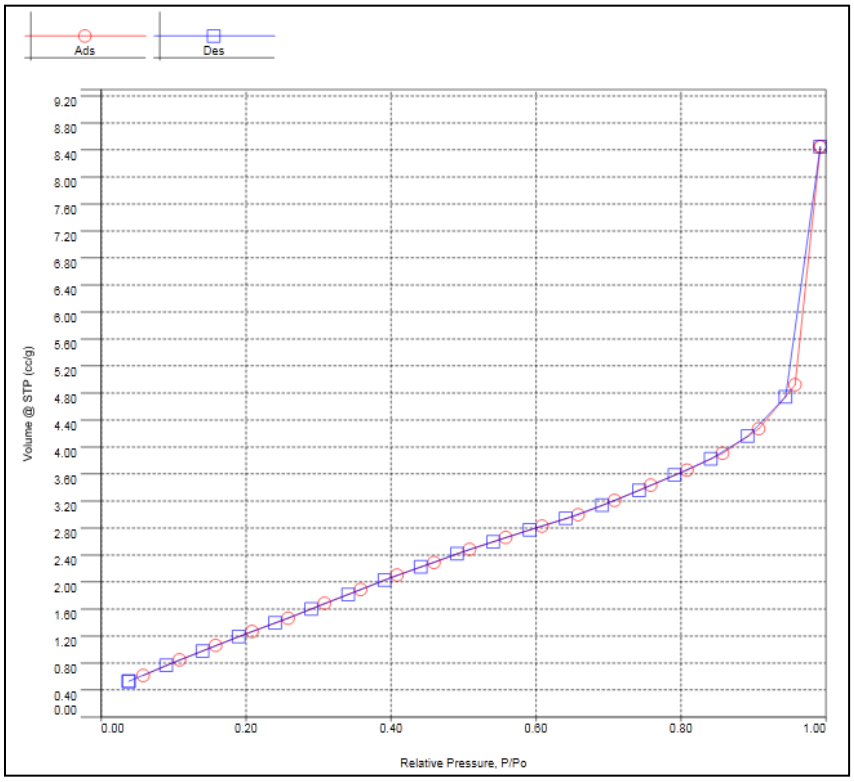

Figure 33 Isotherm for an alumina sample without ice, fired at 1500˚C

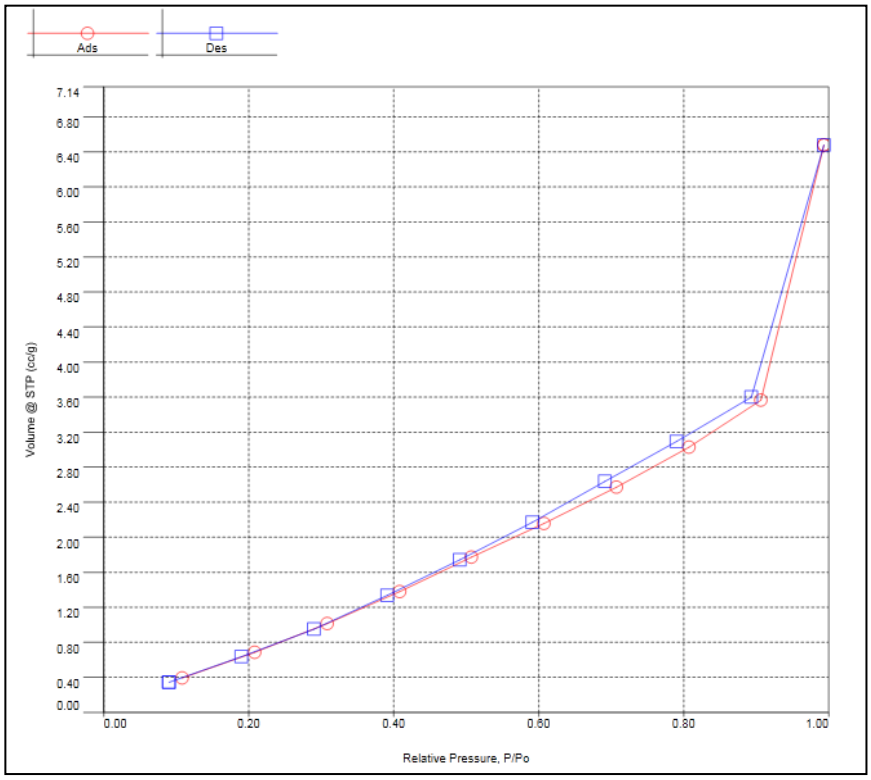

Figure 34 Isotherm for an alumina sample prepared with 43 vol% small spherical ice, frozen in a freezer, and fired at 1500˚C.

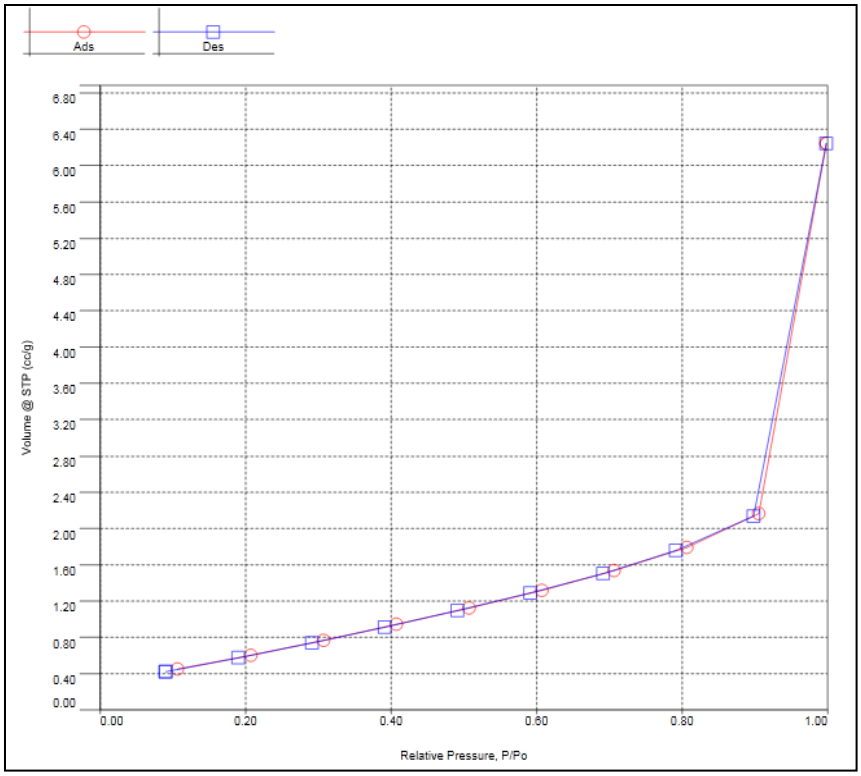

Figure 35 Isotherm for alumina sample with 75 vol% ice, fired at 1500˚C

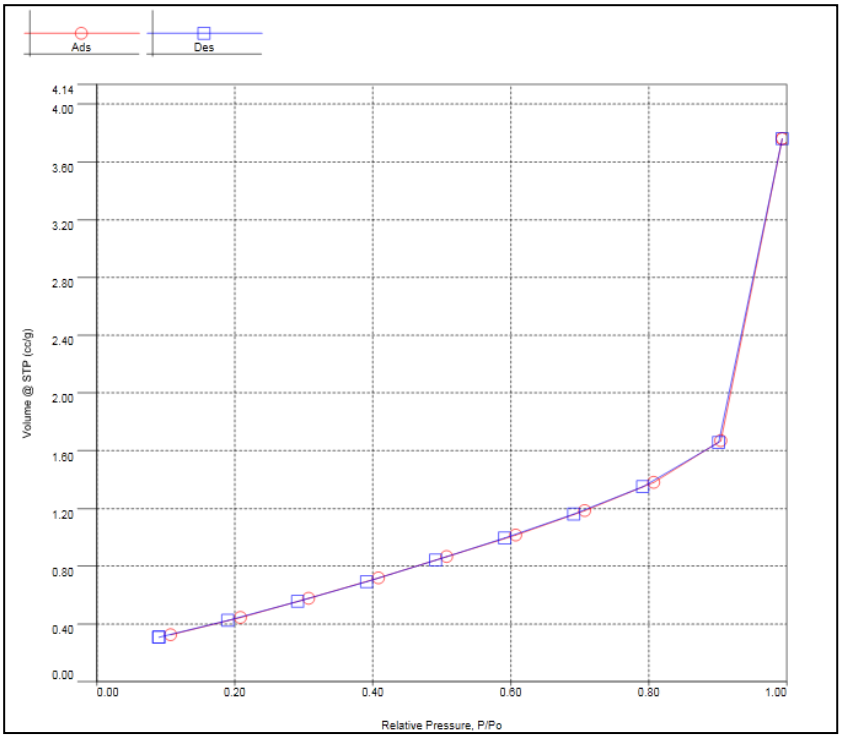

Figure 36 Isotherm for alumina sample with 43 vol% small spherical ice, liquid nitrogen frozen, and fired at 1500 ˚C

4.5.2 Pore Size Distributions

Pore size distribution graphs obtained using the BJH desorption method are shown below in figures 38-41. These figures plot the cumulative pore volume, V(r) in red, and change in pore volume, dV(r) in blue, as a function of pore radius (Å). Figure 37 represents the pore size distribution for the control sample without ice. The cumulative volume of pores spanning a range of approximately 18-800Å reaches 0.012 cc/g.. Both the samples with 43 and 75 vol% small spherical ice that were frozen in a freezer reached a cumulative pore volume of about 0.010 cc/g (seen in Figures 38 and 39). Figure 40 indicates a significantly smaller cumulative pore volume in the range of 18-800Å. This sample was quickly frozen in liquid nitrogen and exhibits a cumulative pore volume of only 0.005 cc/g.

All of these cumulative pore volumes are quite small comparative to the overall size of the sample. Also, the larger pore sizes contribute the most toward the overall pore volumes for each sample analyzed.

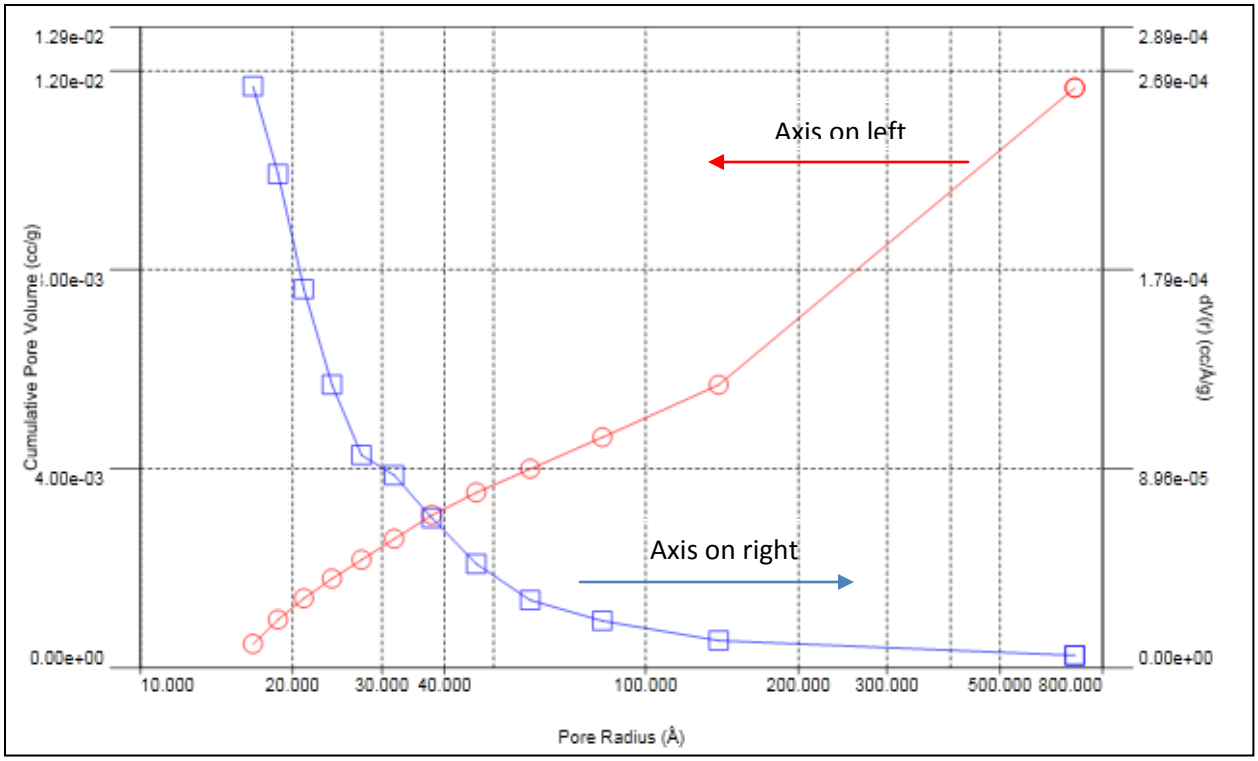

Figure 37 Pore size distribution for alumina sample with no ice, sintered at 1500˚C.

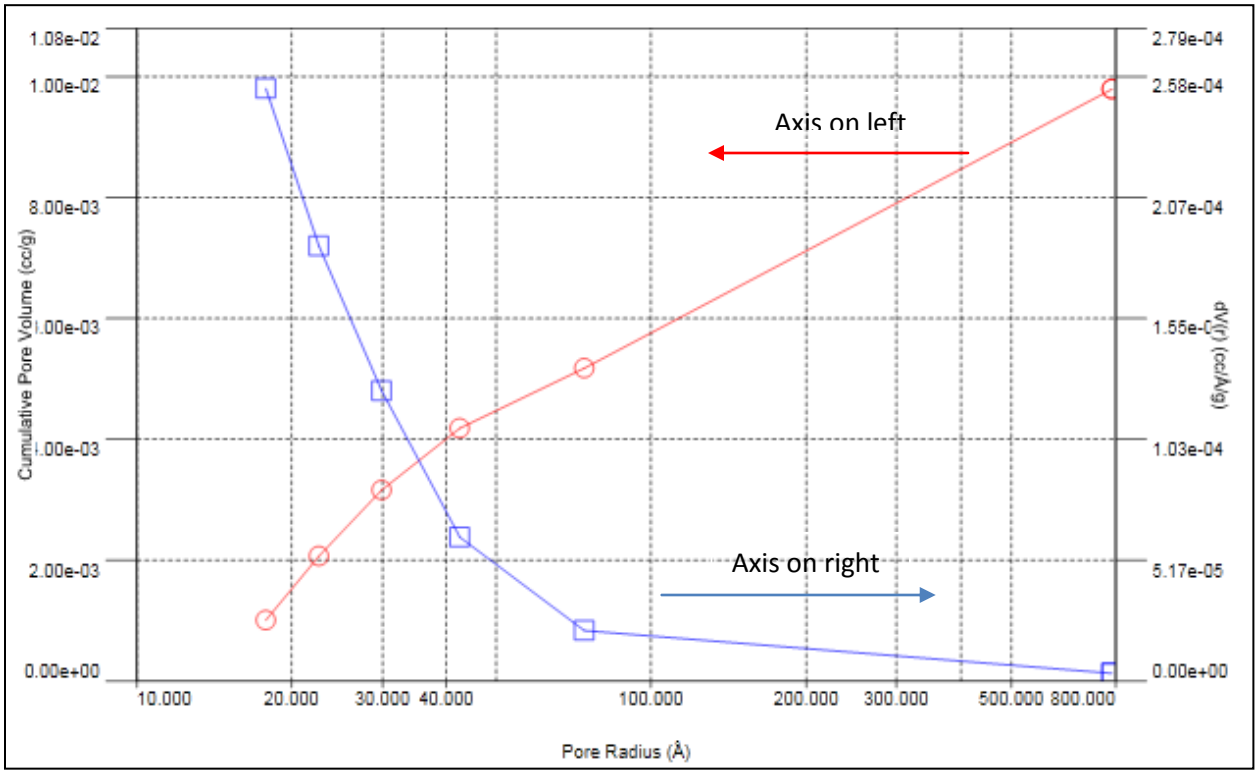

Figure 38 Pore size distribution for an alumina sample prepared with 43 vol% small spherical ice and sintered at 1500˚C.

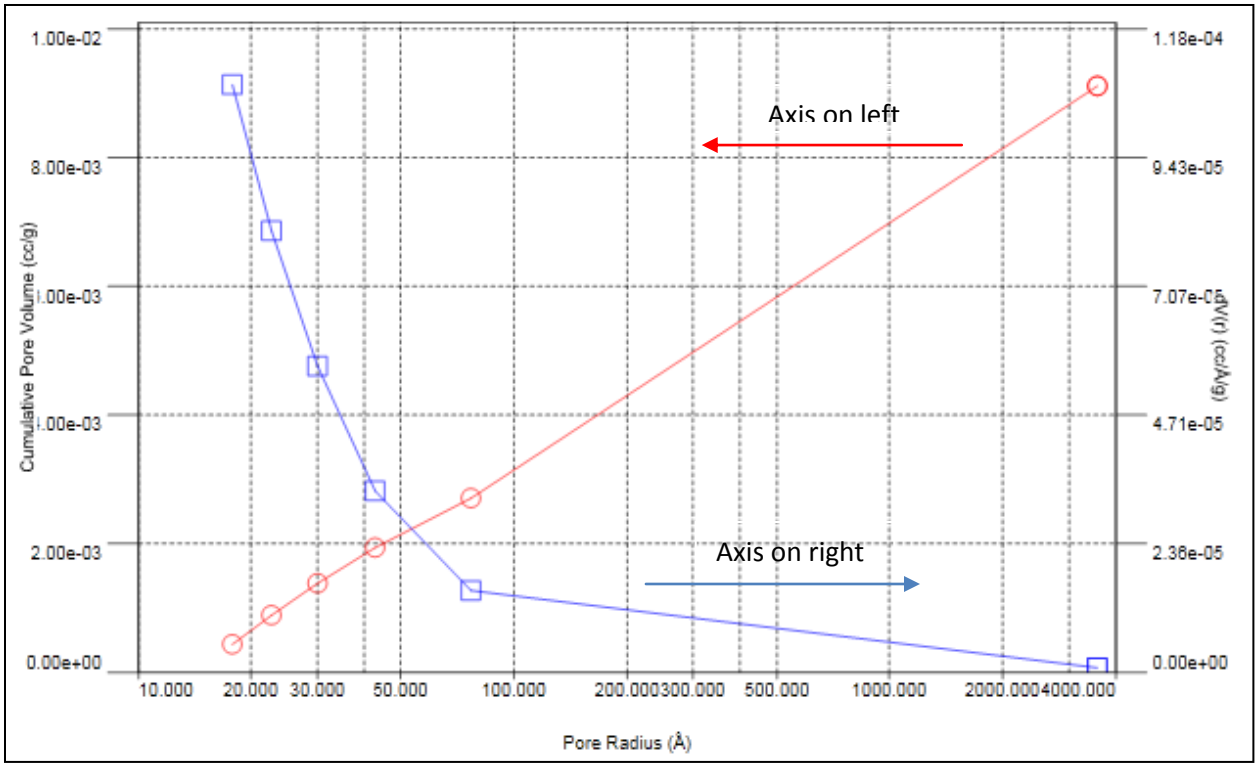

Figure 39 Pore size distribution for alumina sample with 75 vol% ice, fired at 1500˚C

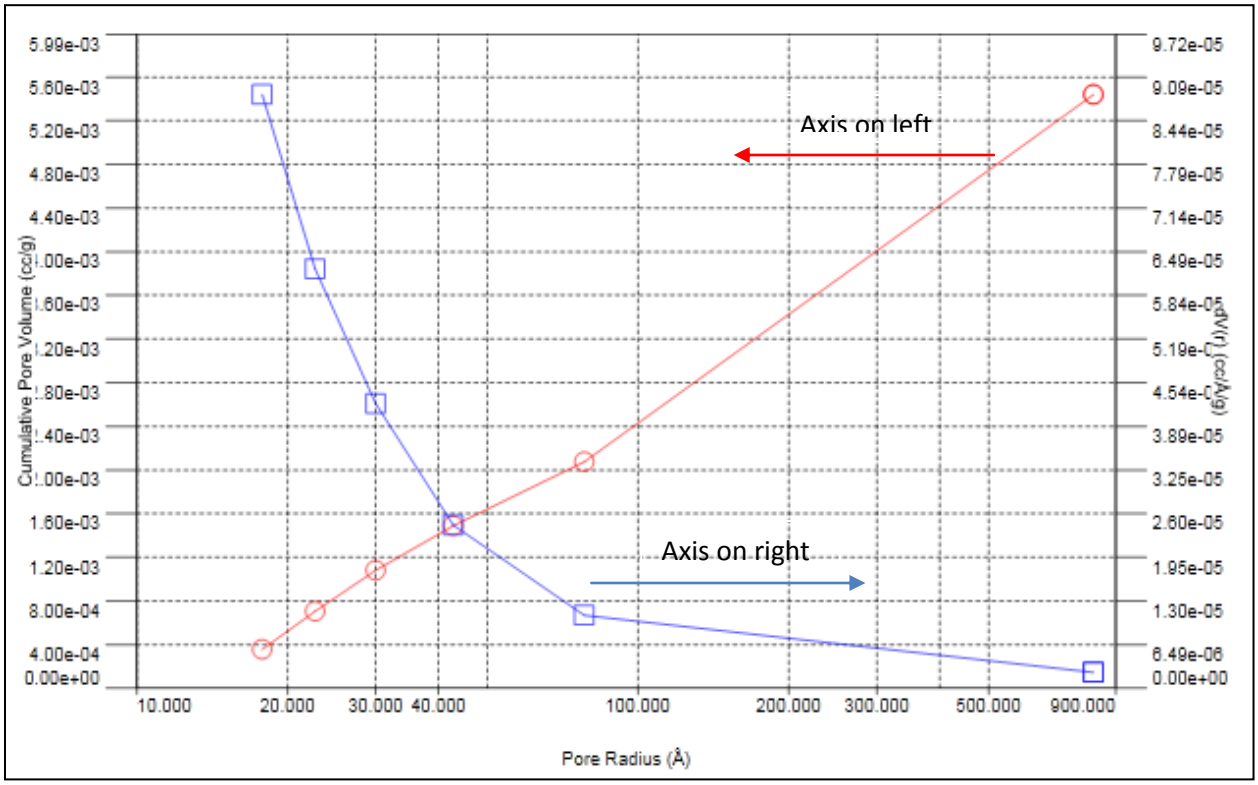

Figure 40 Pore size distribution for alumina sample frozen in liquid nitrogen fired at 1500˚C

Table 7 summarizes the surface areas and pore volumes generated by gas sorption analysis for the four different samples that were tested.

Table 7 Surface areas and pore volumes measured by gas sorption

Sample	Ice Type	Vol% Ice	Freezing Method	T_{sinter} (˚C)	Surface Area (m^2/g)	Pore Volume (cc/g)
A 2.4	Small Spherical	43	Freezer	1500	3.669	.010
A 2.6	Small Spherical	43	Liquid nitrogen	1500	1.384	.005
A 4.1	Small Spherical	75	Freezer	1500	1.721	.009
A C.1	None	0	Freezer	1500	3.465	.012

Chapter 5. Discussion

This chapter is intended to discuss and analyze the results presented in Chapter 4. The overall success of the process and ability to control the porosity using ice particles as PFAs is discussed. This chapter also addresses the issues concerning the scale of the process and what would need to be done to feasibly perform these steps for large scale production in an industrial setting.

5.1 Volume Shrinkage

5.1.1 Volume Shrinkage during Drying

During the initial stages of this study, it was apparent that alumina samples were subjected to a significant amount of shrinkage during the drying process. This volume shrinkage is most likely the result of pore collapse as ice melts and is removed from the sample. As ice melts from a green body, there is nothing present to support the ceramic particles surrounding the ice, and so, pores will begin to collapse, filling in the space once held by ice. This will decrease the overall volume of the sample as well as the amount of porosity in the final structure. As seen in Figure 12, samples with more ice experienced higher amounts of shrinkage during drying and the sample without ice experienced comparatively little shrinkage. The sample with 75 vol% ice was reduced to only 20% of its initial size.

If a component needed to be manufactured to specific dimensions, volume shrinkage would present a big problem for this processing technique. However, many manufacturing processes do not require net shape formation because parts can usually be machined to the desired size after firing., In these cases, volume shrinkage would not be an issue.

The agarose gelling agent was introduced to this study in an attempt to prevent volume shrinkage, especially for samples with large amounts of ice. Agarose, specifically, was chosen because it is a binder which gels upon cooling. It was hoped that upon introduction to the ice particles, the agarose would locally gel within the solid suspension, immediately setting the structure around the ice and maintaining

that pore structure throughout the drying process. This quick polymerization setting technique would have prevented the volume shrinkage from occurring during drying.

Results indicate that the addition of agarose did no help in preventing pore collapse and volume shrinkage during drying. It is believed that the low temperature of ice introduced to the alumina/agarose slurry may interfere with agarose gelling, preventing successful gel formation until the sample warms up. The ice particles introduced to the slurry had just been removed from a dewar liquid nitrogen and their temperature was on the order of -100˚C. It is noted that the alumina/agarose sample prepared without any ice was able to successfully gel within 1 or 2 minutes of sitting in the mold. This quick gellation was not observed in samples prepared with ice particles.

The alumina/agarose preparation method could also be improved to prevent the quick gellation of the agarose solution. In this experiment, the alumina slurry was mixed at room temperature, while the agarose solution alone was heated to 90˚C. It is possible that better gelling could have been obtained had both the alumina slurry and agarose solution been mixed and heated together at 90˚C. This would slow down the rate that the agarose would cool to gelling temperature, because only cold part of the slurry mixture would be the ice particles.

5.1.2 Volume Shrinkage during Sintering

Sintering temperature strongly affected the amount of shrinkage and densification of components during firing, as was expected with solid-state sintering. As described in section 2.4, higher sintering temperatures promote the mechanisms which lead to densification of the component. The densification is a result of particle transport to the neck and causes the overall volume of a component to be reduced in size. This volume reduction is clearly visible in Figure 13.

5.2 Porosity Measurements

5.2.1 Porosity vs. Volume % Ice Added to Slurry

The presence of porosity in control samples which did not contain any ice indicates that there are other sources of porosity in this process besides the PFA added to the slurries. This porosity most likely arises from the packing density of the ceramic powder particles and sintering schedule used. As described in section 2.2.1, porous ceramics can be created by sintering a loosely packed ceramic powder. In this study, the powders were not selected or processed such that they would form a fully dense body without the addition of a PFA. Secondly, the samples were not sintered at an extremely high temperature or for an amount of time that would allow for dense component formation. Porosity levels almost doubled between samples with 0 vol% ice and 43 vol% ice. These samples were processed in exactly the same way, and so this increase in porosity can only be accounted for by the addition of ice to the alumina slurry.

This process has a limited amount of control over the amount of porosity that can be made in a sample. This is because there is a relatively high degree of variation in porosity measurements for samples containing a certain vol% ice. The 95% confidence interval was typically around ± 5% from the sample group mean. This relatively high variation is why samples with 43 and 56 vol% ice were not found to have statistically different porosity levels. In order to be able to hone in on more precise porosity values, this process would have to be further developed for higher degrees of control.

The volume of ice that was added to a slurry did not exactly translate to the volume of porosity found in the final structure. Table 8 summarizes porosity data from Figure 14, including vol% ice added to the slurry, total % porosity found in the final sample, and the difference between the two.

Table 8 Difference between vol% ice and % total porosity

Vol% Ice	% Total Porosity	Difference
0	30	30
43	58	15
56	68	13
75	75	0

Samples prepared without ice had porosity levels that were 30% higher than the volume of ice used. This number decreases as more ice is added to the slurry. A constant amount of porosity is consistent with the packing of the ceramic particles and sintering schedule (porosity seen in the control sample without ice). It is believed that at some point, the limit of this process will be reached, and the addition of more ice will no longer produce higher levels of porosity. This is most likely a result of pore collapsing as described above. Samples using more ice appear to be more susceptible to pore collapse.

5.2.2 ***Porosity vs. Sintering Temperature***

Particle transport and necking cause pores to close up during the solid-state sintering process as Figures 16-18 indicate a strong decrease in porosity as sintering temperatures increase. An increase from 1300˚C to 1500˚C caused a significant decrease in porosity, meaning particle transport rates were higher at the higher temperature. The rate of change between 1500˚C and 1600˚C was not enough to cause further decreases in porosity because no significant changes were observed between samples treated at these temperatures. Particle transport during the sintering process appears to close up the open pores in the sample. This is evidenced by the fact that the total amount of porosity is decreasing, however amounts of closed porosity remain relatively constant or (in the case of the sample frozen in liquid nitrogen) actually increase as higher sintering temperatures are used.

The size of the ice particles used as PFA's did not change the total amount of porosity observed in samples, however it did change the type of porosity. Samples that were prepared with smaller spherical shaped ice particles displayed higher amounts of closed porosity than samples which used the larger blended ice particles. The smaller spherical ice particles were more likely isolated from one another within the green bodies and did not have as much interconnectivity to open the pores to the environment. It appears that larger ice particles are more likely to touch one another in a green body, producing higher amounts of open porosity.

Samples that were frozen in liquid nitrogen before drying had significantly lower porosities than samples that were frozen in a freezer. As higher sintering temperatures were used, porosity type actually

switched from a majority of open porosity at 1300˚C to a majority of closed porosity at 1600˚C. The particle transport is working to close up previously opened pores. At this point, the reasoning behind the the lower porosities and the switch from open to closed porosity seen in samples frozen in liquid nitrogen is not understood. It may be that pores in these samples are smaller to begin with, as smaller open pores are more quickly closed up during sintering than larger open pores. The smaller pores would also explain the lower % total porosity seen in these samples. The reason why pores would be smaller after being frozen in liquid nitrogen is not obvious.

5.3 Optical Microscopy

Pores observed in the optical microscope images matched well with the ice particles used to create them. Pore widths observed in the optical images were slightly smaller than the sizes of the spherical ice particles, however the shape of the ice particles appears to have translated well into the ceramic sample. Sintering can account for the slightly smaller pore size. As described in section 2.6, large pores will typically shrink by the same amount the entire sample shrinks. Pore collapse during drying also accounts for existing pores smaller than the PFA used to create them. The presence of interconnected pores seen in Figure 25 is interesting. Interconnected porosity was not uniformly observed in all samples, meaning it is not well controlled with the current processing route used in this study.

5.4 Scanning Electron Microscopy

Two types of porosities were observed with the SEM. Pores on the order of 0.5 microns were seen surrounding the ceramic particles at high magnification levels. The optical images of the ice particles shown in section 4.3.1 confirm this small porosity arises from the packing of alumina particles in the mold and not the ice particles. The ice particles are much too big to create such tiny pores. These pores were quickly eliminated at higher sintering temperatures as necking between particles occurred and

grains grew larger. The alumina control sample was found to only have this first, smaller type of porosity present,

The second type of porosity encountered was anywhere on the order of 20-200μm. This size range is consistent with the size range of the small spherical particles imaged in Figure 20. Samples that were prepared with the large spherical ice particles were imaged in SEM, however the pores were so large, that the SEM could not accurately depict them and so they are not presented here. The optical images offer the best understanding of the large pores present in these samples. Pores seen in the SEM images tend to be relatively round in shape. Some elongated pores can be found in the sample. It is possible that these pores were formed by two spherical ice particles that were in contact with one another in the frozen green body. Pore interconnectivity was seen throughout the sample prepared with 43 vol% ice and frozen in the freezer.

The sample that was frozen in liquid nitrogen before drying displayed a different porous microstructure. The sparsely distributed pores do not appear to touch one another very often and this observation correlates with the porosity measured from Archimedes method. Samples that were frozen in liquid nitrogen were found to have significantly higher amounts of closed porosity than their counterparts that were frozen in a freezer and this closed porosity is visible in the SEM images. Pore sizes and shapes seen in the alumina/agarose sample are consistent with the pore sizes and shapes also formed by the small spherical ice in other samples.

5.5 Gas Sorption

5.5.1 Isotherm Plots

The shape of the isotherm curve in Figure 36 indicates a type II sorption isotherm. Components exhibiting type II isotherms are characterized by either no porosity or by a majority of macroporosity (greater than 50 nm). The limitations of the gas sorption method are exemplified here as the method is able to indicate that large pores are present, but it cannot distinguish the size or relative amount of these larger pores. In gas sorption a macropore is "seen" by the adsorbate as a flat surface and cannot be

detected [58]. The sample prepared frozen in liquid nitrogen can therefore be characterized as macroporous. We know porosity exists in these samples from Archimedes porosity testing, and the linear isotherms indicate that none of this porosity falls below 50 nm in size.

Figures 33-35 on the other hand, depict type IV isotherms. The slight hysteresis in these figures is characteristic of a mesoporous material and is produced from the occurrence of pore condensation during adsorption [58]. Mesopores are defined as pores with a width falling between 2 and 50 nm. The hysteresis is not strong for either of these samples; however the shape of the hysteresis provides information on the relative shape of the pores detected by sorption. The International Union of Pure and Applied Chemistry (IUPAC) has defined 4 classes of hysteresis loops seen to the right in Figure 41.

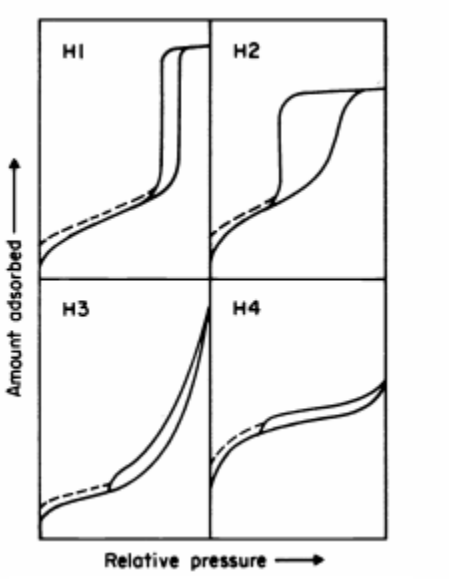

Figure 41 IUPAC classifications of hysteresis loops [59]

The hysteresis loops seen in Figures 33 and 35 are clearly type H1 hysteresis loops. As described by Lowell et al., "type H1 is often associated with porous materials consisting of well-defined cylindrical-like pore channels…" [58]. The hysteresis depicted in Figure 35 appears to be somewhat in between a type H1 and a type H3 classification. H3 classified loops are often associated with slit-shaped pores [58]. Although the amount of mesopores in these samples is rather low, they seem to be well-defined in terms of shape and uniformity.

5.5.2 Pore Size Distributions, Surface Area, and Pore Volumes

The pore size distributions indicate that the majority of pores present in these samples are larger than the range detected by gas sorption. No peaks were observed in the covered ranges and increases in the cumulative pore volume increased in size for larger pore radii. The existence of the peaks is confirmed by the presence of very small pores on the order of 700 angstroms as observed in the SEM images. These pores most likely result from the packing of the ceramic powder particles and this is the

reason why no significant difference is observed between the control sample without ice and the sample that was prepared with 43 vol% ices. The volume of pores present in the sample frozen in liquid nitrogen was much smaller than the other 3 samples that were tested.

5.6 Industrial Feasibility

In addition to introducing the use of ice particles as a pore-forming agent, one of the main purposes of this study was to prove the feasibility of this process within an industrial setting. Samples presented here were made in small scale within a laboratory, and a few modifications would need to be made in order for this process to succeed in an industrial manufacturing setting.

In this experiment, spherical ice particles were hand made on an as needed basis. A typical spray nozzle was used to spray water into a dewar of liquid nitrogen until enough ice had collected at the bottom to be added to a sample. It is understood that this method would become completely impractical if large quantities of ice were needed. The following method is proposed for the creation of ice particles. A tube with pressurized water flow can be fixed above a large dewar of liquid nitrogen. Nozzles on the tube allow for a consistent spray of water into the dewar. More nozzles can be used to allow for faster production of ice. The size of the nozzle as well as the pressure within the tube can be changed to control the size of ice particles that are desired. This idea is sketched out above in Figure 42.

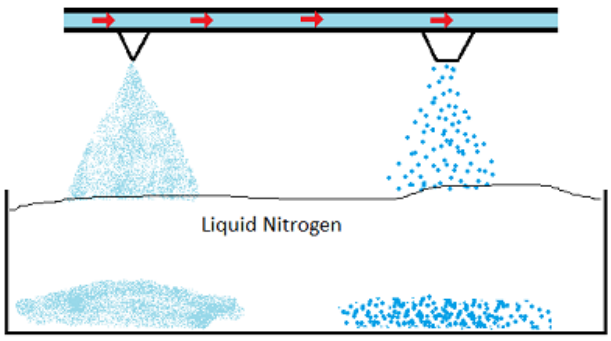

Figure 42 Sketch of ice particle fabrication for large scale industrial use

Chapter 6. Conclusions

Limitations of current porous ceramic processing methods include high cost, environmental unfriendliness, and most importantly, lack of control over pore size, shape and uniformity. These current processing methods often fail when met with the challenges of a precise and complex porous design required by highly advanced applications. This study presented a new route to porous ceramics that has the potential to be low cost, environmentally friendly and allow for a high degree of control over the types of pores it creates. Porous alumina was successfully prepared with the novel use of ice particles as a pore forming agent. The effect of ice particle size, amount of ice used, presence of a gelling agent, freezing rate, and sintering temperature on porosity and microstructure were analyzed.

In this study, alumina samples were prepared with pores ranging from 20μm to 3mm in diameter. Porosity levels ranged from 30% to 75%. Amount of porosity was able to be controlled through the amount of ice particles added to the ceramic slurry as well as the firing temperature of the green body. The size and shape of ice particles were able to be changed based on the size and shape of the ice particles that were made.

While the total amount of porosity and the shape of the pores was able to be controlled within this study, more work will need to be done to address other factors that were not able to be controlled in this study. Interconnected porosity, for example, was randomly seen in various samples. Samples that were frozen in liquid nitrogen displayed vastly different pore microstructures and lower porosity levels and the reasoning behind this is currently unknown. Volume shrinkage and pore collapse during the drying process appear to be one of the major issues concerning this process. An organic gelling agent was used in an attempt to prevent drying shrinkages, however, it was unsuccessful.

This study aimed to prove the feasibility of using ice particles as pore forming agents. Although more work is needed to gain better control over porosity, the simplicity of this process makes it extremely appealing over other current fabrication methods.

6.1 Future Work

One important future study would focus on the mechanical properties of porous parts made via this method. In order to fully confirm the feasibility of this process to be used in an industrial setting, the mechanical properties, such as hardness and flexural strength, of parts would need to be confirmed and compared with reported mechanical properties existing in literature.

In order to combat the issues involving volume shrinkage, future work would focus on finding an appropriate slurry additive to set the structure of the ceramic powder particles around the ice within the green body. Although agarose did not work in this study, more work could focus on finding a gelling agent which may be able to endure the extremely cold ice particles it will come in contact with. The agarose method could also be altered to slow down the gelling rate as described in section 5.1.1. UV-crosslinkers may be another option and a study that works on finding an ideal setting agent would be advantageous to this process.

Finally, it would be interesting to try and use ice particles as a pore forming agent in a metallic or a polymeric system. This would help to demonstrate the dynamic ability of this process to create pores in just about any system.

References

1. Damoah, L.N.W. and L. Zhang, *AlF3 reactive Al2O3 foam filter for the removal of dissolved impurities from molten aluminum: Preliminary results.* Acta Materialia, 2011. **59**(3): p. 896-913.

2. Jo, Y.M., R.B. Hutchison, and J.A. Raper, *Characterization of ceramic composite membrane filters for hot gas cleaning.* Powder Technology, 1997. **91**(1): p. 55-62.

3. Julbe, A., D. Farrusseng, and C. Guizard, *Porous ceramic membranes for catalytic reactors -- overview and new ideas.* Journal of Membrane Science, 2001. **181**(1): p. 3-20.

4. Green, D.J., *Porous Ceramics including Fibrous Insulation, Structure and Properties of*, in *Encyclopedia of Materials: Science and Technology*, K.H.J. Buschow, et al., Editors. 2001, Elsevier: Oxford. p. 7762-7764.

5. Tang, C.-W., et al., *Production of synthetic lightweight aggregate using reservoir sediments for concrete and masonry.* Cement and Concrete Composites, 2011. **33**(2): p. 292-300.

6. Rezwan, K., et al., *Biodegradable and bioactive porous polymer/inorganic composite scaffolds for bone tissue engineering.* Biomaterials, 2006. **27**(18): p. 3413-3431.

7. Takahashi, M., et al., *Opportunities of porous ceramics fabricated by gelcasting in mitigating environmental issues.* Journal of the European Ceramic Society, 2009. **29**(5): p. 823-828.

8. Chen, S.-L., et al., *Large pore heavy oil processing catalysts prepared using colloidal particles as templates.* Catalysis Today, 2007. **125**(3-4): p. 143-148.

9. Wen, Z.-H., et al., *Preparation of porous ceramics with controllable pore sizes in an easy and low-cost way.* Materials Characterization, 2008. **59**(9): p. 1335-1338.

10. Manjooran, N.J. and G.R. Pickrell, *Biologically self-assembled porous polymers.* Journal of Materials Processing Technology, 2005. **168**(2): p. 225-229.

11. Gregorová, E. and W. Pabst, *Porous ceramics prepared using poppy seed as a pore-forming agent.* Ceramics International, 2007. **33**(7): p. 1385-1388.

12. Gregorová, E., et al., *Porous alumina ceramics prepared with wheat flour.* Journal of the European Ceramic Society, 2010. **30**(14): p. 2871-2880.

13. Bai, J., *Fabrication and properties of porous mullite ceramics from calcined carbonaceous kaolin and [alpha]-Al2O3.* Ceramics International, 2010. **36**(2): p. 673-678.

14. Dressler, M., et al., *Burnout behavior of ceramic coated open cell polyurethane (PU) sponges.* Journal of the European Ceramic Society, 2009. **29**(16): p. 3333-3339.

15. Kamijo, T., et al., *High-temperature micro catalytic combustor with Pd/nano-porous alumina.* Proceedings of the Combustion Institute, 2009. **32**(2): p. 3019-3026.

16. Nandi, B.K., R. Uppaluri, and M.K. Purkait, *Preparation and characterization of low cost ceramic membranes for micro-filtration applications.* Applied Clay Science, 2008. **42**(1-2): p. 102-110.

17. Zhang, H.L., J.-F. Li, and B.-P. Zhang, *Microstructure and electrical properties of porous PZT ceramics derived from different pore-forming agents.* Acta Materialia, 2007. **55**(1): p. 171-181.

18. Wang, Q., et al., *Effects of pore shape and porosity on the properties of porous LNKN ceramics as bone substitute.* Materials Chemistry and Physics, 2008. **109**(2-3): p. 488-491.

19. Yoon, B.-H., et al., *Aligned porous alumina ceramics with high compressive strengths for bone tissue engineering.* Scripta Materialia, 2008. **58**(7): p. 537-540.

20. D.A. Hirschfeld, T.K.L., and D.M. Liu, *Processing of Porous Oxide Ceramics.* Key Engineering Materials, 1996. **115**: p. 65-80.

21. Li, S. and N. Li, *Effects of composition and temperature on porosity and pore size distribution of porous ceramics prepared from Al(OH)3 and kaolinite gangue.* Ceramics International, 2007. **33**(4): p. 551-556.

22. Galassi, C., *Processing of porous ceramics: Piezoelectric materials.* Journal of the European Ceramic Society, 2006. **26**(14): p. 2951-2958.

23. Kim, J.G., J.H. Sim, and W.S. Cho, *Preparation of porous (Ba,Sr)TiO3 by adding corn-starch.* Journal of Physics and Chemistry of Solids, 2002. **63**(11): p. 2079-2084.

24. Takao, Y., et al., *Microstructure of alumina compact body made by slip casting.* Journal of the European Ceramic Society, 2002. **22**(4): p. 397-401.

25. Tsetsekou, A., C. Agrafiotis, and A. Milias, *Optimization of the rheological properties of alumina slurries for ceramic processing applications Part I: Slip-casting.* Journal of the European Ceramic Society, 2001. **21**(3): p. 363-373.

26. Ainsley, C. and H. Gong, *Precision sintering of slip cast components.* Journal of Materials Processing Technology, 1999. **95**(1-3): p. 201-209.

27. Laurie, J., et al., *Colloidal suspensions for the preparation of ceramics by a freeze casting route.* Journal of Non-Crystalline Solids, 1992. **147-148**: p. 320-325.

28. Jing, L., et al., *The controllable microstructure of porous Al2O3 ceramics prepared via a novel freeze casting route.* Ceramics International, 2010. **36**(8): p. 2499-2503.

29. Ren, L., Y.-P. Zeng, and D. Jiang, *Preparation of porous TiO2 by a novel freeze casting.* Ceramics International, 2009. **35**(3): p. 1267-1270.

30. Han, J., et al., *Highly porous ZrO2 ceramics fabricated by a camphene-based freeze-casting route: Microstructure and properties.* Journal of the European Ceramic Society, 2010. **30**(1): p. 53-60.

31. Ye, F., et al., *Pore structure and mechanical properties in freeze cast porous Si3N4 composites using polyacrylamide as an addition agent.* Journal of Alloys and Compounds, 2010. **506**(1): p. 423-427.

32. Moritz, T. and H.-J. Richter, *Ice-mould freeze casting of porous ceramic components.* Journal of the European Ceramic Society, 2007. **27**(16): p. 4595-4601.

33. Hu, L., et al., *Control of pore channel size during freeze casting of porous YSZ ceramics with unidirectionally aligned channels using different freezing temperatures.* Journal of the European Ceramic Society, 2010. **30**(16): p. 3389-3396.

34. Zhang, Y., et al., *Freeze casting of aqueous alumina slurries with glycerol for porous ceramics.* Ceramics International, 2010. **36**(2): p. 617-621.

35. Ye, F., et al., *Effect of solid content on pore structure and mechanical properties of porous silicon nitride ceramics produced by freeze casting.* Materials Science and Engineering: A, 2011. **528**(3): p. 1421-1424.

36. Deville, S., E. Saiz, and A.P. Tomsia, *Freeze casting of hydroxyapatite scaffolds for bone tissue engineering.* Biomaterials, 2006. **27**(32): p. 5480-5489.

37. Yang, T.Y., et al., *Porous mullite composite with controlled pore structure processed using a freeze casting of TBA-based coal fly ash slurries.* Resources, Conservation and Recycling, 2010. **54**(11): p. 816-820.

38. Zhang, Y., K. Zuo, and Y.-P. Zeng, *Effects of gelatin addition on the microstructure of freeze-cast porous hydroxyapatite ceramics.* Ceramics International, 2009. **35**(6): p. 2151-2154.

39. Yang, J., J. Yu, and Y. Huang, *Recent developments in gelcasting of ceramics.* Journal of the European Ceramic Society, 2011. **In Press, Corrected Proof**.

40. Gu, Y., et al., *Porous YSZ ceramics by water-based gelcasting.* Ceramics International, 1999. **25**(8): p. 705-709.

41. Meng, G., et al., *Preparation of porous ceramics by gelcasting approach.* Materials Letters, 2000. **45**(3-4): p. 224-227.

42. Omatete, O.O., M.A. Janney, and R.A. Strehlow, *Gelasting- a new ceramic forming process.* American Ceramic Society Bulletin, 1991. **70**.

43. Janney, M.A., et al., *Development of Low-Toxicity Gelcasting Systems.* Journal of the American Ceramic Society, 1998. **81**(3): p. 581-591.

44. Potoczek, M., *Gelcasting of alumina foams using agarose solutions.* Ceramics International, 2008. **34**(3): p. 661-667.

45. Ewais, E.M.M. and A. Safari, *Gelation of water-based PZT slurries in the presence of ammonium polyacrylate using agarose.* Journal of the European Ceramic Society, 2010. **30**(16): p. 3425-3434.

46. Pourcel, F., et al., *Criterion for crack initiation during drying: Alumina porous ceramic strength improvement.* Powder Technology, 2007. **172**(2): p. 120-127.

47. Skansi, D. and S. Tomas, *Microwave drying kinetics of a clay-plate.* Ceramics International, 1995. **21**(3): p. 207-211.

48. Barati, A., M. Kokabi, and M.H.N. Famili, *Drying of gelcast ceramic parts via the liquid desiccant method.* Journal of the European Ceramic Society, 2003. **23**(13): p. 2265-2272.

49. Lin, S.I.E., *Near-net-shape forming of zirconia optical sleeves by ceramics injection molding.* Ceramics International, 2001. **27**(2): p. 205-214.

50. Sato, T., T. Besshi, and M. Matsui, *A new near net-shape forming process for alumina.* Journal of Materials Processing Technology, 1998. **79**(1-3): p. 125-132.

51. Ganesh, I., et al., *Hydrolysis-induced aqueous gelcasting for near-net shape forming of ZTA ceramic composites.* Journal of the European Ceramic Society, 2009. **29**(8): p. 1393-1401.

52. Bocanegra-Bernal, M.H. and B. Matovic, *Dense and near-net-shape fabrication of Si3N4 ceramics.* Materials Science and Engineering: A, 2009. **500**(1-2): p. 130-149.

53. Gilissen, R., et al., *Gelcasting, a near net shape technique.* Materials & Design, 2000. **21**(4): p. 251-257.

54. Yet-Ming Chiang, D.B.I., W. David Kingery, *Physical Ceramics: Principles for Ceramic Science and Engineering*. 1997: John Wiley & Sons.

55. Lame, O., et al., *In situ microtomography investigation of metal powder compacts during sintering.* Nuclear Instruments and Methods in Physics Research Section B: Beam Interactions with Materials and Atoms, 2003. **200**: p. 287-294.

56. Lange, E.B.S.a.F.F., *Densification of Large Pores: I, Experiments.* J. Am. Ceram. Soc., 1992. **75**(9): p. 2498-2508.

57. Garrido, L.B., et al., *Effect of starch filler content and sintering temperature on the processing of porous 3Y-ZrO2 ceramics.* Journal of Materials Processing Technology, 2009. **209**(1): p. 590-598.

58. Lowell, S., et al., *Characterization of Porous Solids and Powders: Surface Area, Pore Size, and Density*. 2004: Kluwer Academic Publishers.

59. Sing, K.S.W., et al., *Reporting Physisorption Data For Gas/Solid Systems.* Pure & Appl. Chem., 1985. **57**(4): p. 603-619.

Appendix A. Permissions

A.1 Elsevier

ELSEVIER LICENSE
TERMS AND CONDITIONS
Jun 13, 2011

This is a License Agreement between Samantha Smith ("You") and Elsevier ("Elsevier") provided by Copyright Clearance Center ("CCC"). The license consists of your order details, the terms and conditions provided by Elsevier, and the payment terms and conditions.

All payments must be made in full to CCC. For payment instructions, please see information listed at the bottom of this form.

Supplier	Elsevier Limited The Boulevard,Langford Lane Kidlington,Oxford,OX5 1GB,UK
Registered Company Number	1982084
Customer name	Samantha Smith
Customer address	311 Hunt Club Rd. Blacksburg, VA 24060
License number	2687200769938
License date	Jun 13, 2011
Licensed content publisher	Elsevier
Licensed content publication	Journal of Materials Processing Technology
Licensed content title	Precision sintering of slip cast components
Licensed content author	C. Ainsley, H. Gong
Licensed content date	15 October 1999
Licensed content volume number	95
Licensed content issue number	1-3
Number of pages	9
Start Page	201
End Page	209
Type of Use	reuse in a thesis/dissertation
Portion	figures/tables/illustrations
Number of figures/tables/illustrations	1
Format	both print and electronic
Are you the author of this Elsevier article?	No
Will you be translating?	No
Order reference number	
Title of your thesis/dissertation	Novel preparation of porous alumina using ice particles as pore-forming agents
Expected completion date	Jul 2011
Estimated size (number of pages)	75
Elsevier VAT number	GB 494 6272 12
Permissions price	0.00 USD
VAT/Local Sales Tax	0.0 USD / 0.0 GBP
Total	0.00 USD

Terms and Conditions

INTRODUCTION

1. The publisher for this copyrighted material is Elsevier. By clicking "accept" in connection with completing this licensing transaction, you agree that the following terms and conditions apply to this transaction (along with the Billing and Payment terms and conditions established by Copyright Clearance Center, Inc. ("CCC"), at the time that you opened your Rightslink account and that are available at any time at http://myaccount.copyright.com).

GENERAL TERMS

2. Elsevier hereby grants you permission to reproduce the aforementioned material subject to the terms and conditions indicated.

3. Acknowledgement: If any part of the material to be used (for example, figures) has appeared in our publication with credit or acknowledgement to another source, permission must also be sought from that source. If such permission is not obtained then that material may not be included in your publication/copies. Suitable acknowledgement to the source must be made, either as a footnote or in a reference list at the end of your publication, as follows:

"Reprinted from Publication title, Vol /edition number, Author(s), Title of article / title of chapter,

ELSEVIER LICENSE
TERMS AND CONDITIONS
Jun 13, 2011

This is a License Agreement between Samantha Smith ("You") and Elsevier ("Elsevier") provided by Copyright Clearance Center ("CCC"). The license consists of your order details, the terms and conditions provided by Elsevier, and the payment terms and conditions.

All payments must be made in full to CCC. For payment instructions, please see information listed at the bottom of this form.

Supplier	Elsevier Limited The Boulevard,Langford Lane Kidlington,Oxford,OX5 1GB,UK
Registered Company Number	1982084
Customer name	Samantha Smith
Customer address	311 Hunt Club Rd. Blacksburg, VA 24060
License number	2687201094495
License date	Jun 13, 2011
Licensed content publisher	Elsevier
Licensed content publication	Journal of the European Ceramic Society
Licensed content title	Control of pore channel size during freeze casting of porous YSZ ceramics with unidirectionally aligned channels using different freezing temperatures
Licensed content author	Liangfa Hu, Chang-An Wang, Yong Huang, Chencheng Sun, Sheng Lu, Zijun Hu
Licensed content date	December 2010
Licensed content volume number	30
Licensed content issue number	16
Number of pages	8
Start Page	3389
End Page	3396
Type of Use	reuse in a thesis/dissertation
Intended publisher of new work	other
Portion	figures/tables/illustrations
Number of figures/tables/illustrations	1
Format	both print and electronic
Are you the author of this Elsevier article?	No
Will you be translating?	No
Order reference number	
Title of your thesis/dissertation	Novel preparation of porous alumina using ice particles as pore-forming agents
Expected completion date	Jul 2011
Estimated size (number of pages)	75
Elsevier VAT number	GB 494 6272 12
Permissions price	0.00 USD
VAT/Local Sales Tax	0.0 USD / 0.0 GBP
Total	0.00 USD

Terms and Conditions

INTRODUCTION

1. The publisher for this copyrighted material is Elsevier. By clicking "accept" in connection with completing this licensing transaction, you agree that the following terms and conditions apply to this transaction (along with the Billing and Payment terms and conditions established by Copyright Clearance Center, Inc. ("CCC"), at the time that you opened your Rightslink account and that are available at any time at http://myaccount.copyright.com).

GENERAL TERMS

2. Elsevier hereby grants you permission to reproduce the aforementioned material subject to the

ELSEVIER LICENSE
TERMS AND CONDITIONS
Jun 13, 2011

This is a License Agreement between Samantha Smith ("You") and Elsevier ("Elsevier") provided by Copyright Clearance Center ("CCC"). The license consists of your order details, the terms and conditions provided by Elsevier, and the payment terms and conditions.

All payments must be made in full to CCC. For payment instructions, please see information listed at the bottom of this form.

Supplier	Elsevier Limited The Boulevard,Langford Lane Kidlington,Oxford,OX5 1GB,UK
Registered Company Number	1982084
Customer name	Samantha Smith
Customer address	311 Hunt Club Rd. Blacksburg, VA 24060
License number	2687201347599
License date	Jun 13, 2011
Licensed content publisher	Elsevier
Licensed content publication	Nuclear Instruments and Methods in Physics Research Section B: Beam Interactions with Materials and Atoms
Licensed content title	In situ microtomography investigation of metal powder compacts during sintering
Licensed content author	Olivier Lame, Daniel Bellet, Marco Di Michiel, Didier Bouvard
Licensed content date	January 2003
Licensed content volume number	200
Licensed content issue number	
Number of pages	8
Start Page	287
End Page	294
Type of Use	reuse in a thesis/dissertation
Intended publisher of new work	other
Portion	figures/tables/illustrations
Number of figures/tables/illustrations	1
Format	both print and electronic
Are you the author of this Elsevier article?	No
Will you be translating?	No
Order reference number	
Title of your thesis/dissertation	Novel preparation of porous alumina using ice particles as pore-forming agents
Expected completion date	Jul 2011
Estimated size (number of pages)	75
Elsevier VAT number	GB 494 6272 12
Permissions price	0.00 USD
VAT/Local Sales Tax	0.0 USD / 0.0 GBP
Total	0.00 USD

Terms and Conditions

INTRODUCTION

1. The publisher for this copyrighted material is Elsevier. By clicking "accept" in connection with completing this licensing transaction, you agree that the following terms and conditions apply to this transaction (along with the Billing and Payment terms and conditions established by Copyright Clearance Center, Inc. ("CCC"), at the time that you opened your Rightslink account and that are available at any time at http://myaccount.copyright.com).

GENERAL TERMS

2. Elsevier hereby grants you permission to reproduce the aforementioned material subject to the terms and conditions indicated.

3. Acknowledgement: If any part of the material to be used (for example, figures) has appeared in

ELSEVIER LICENSE
TERMS AND CONDITIONS
Jun 13, 2011

This is a License Agreement between Samantha Smith ("You") and Elsevier ("Elsevier") provided by Copyright Clearance Center ("CCC"). The license consists of your order details, the terms and conditions provided by Elsevier, and the payment terms and conditions.

All payments must be made in full to CCC. For payment instructions, please see information listed at the bottom of this form.

Supplier	Elsevier Limited The Boulevard,Langford Lane Kidlington,Oxford,OX5 1GB,UK
Registered Company Number	1982084
Customer name	Samantha Smith
Customer address	311 Hunt Club Rd. Blacksburg, VA 24060
License number	2687201216133
License date	Jun 13, 2011
Licensed content publisher	Elsevier
Licensed content publication	Journal of the European Ceramic Society
Licensed content title	Recent developments in gelcasting of ceramics
Licensed content author	Jinlong Yang, Juanli Yu, Yong Huang
Licensed content date	22 January 2011
Licensed content volume number	n/a
Licensed content issue number	n/a
Number of pages	1
Start Page	0
End Page	0
Type of Use	reuse in a thesis/dissertation
Intended publisher of new work	other
Portion	figures/tables/illustrations
Number of figures/tables/illustrations	1
Format	both print and electronic
Are you the author of this Elsevier article?	No
Will you be translating?	No
Order reference number	
Title of your thesis/dissertation	Novel preparation of porous alumina using ice particles as pore-forming agents
Expected completion date	Jul 2011
Estimated size (number of pages)	75
Elsevier VAT number	GB 494 6272 12
Permissions price	0.00 USD
VAT/Local Sales Tax	0.0 USD / 0.0 GBP
Total	0.00 USD

Terms and Conditions

INTRODUCTION

1. The publisher for this copyrighted material is Elsevier. By clicking "accept" in connection with completing this licensing transaction, you agree that the following terms and conditions apply to this transaction (along with the Billing and Payment terms and conditions established by Copyright Clearance Center, Inc. ("CCC"), at the time that you opened your Rightslink account and that are available at any time at http://myaccount.copyright.com).

GENERAL TERMS

2. Elsevier hereby grants you permission to reproduce the aforementioned material subject to the terms and conditions indicated.

3. Acknowledgement: If any part of the material to be used (for example, figures) has appeared in our publication with credit or acknowledgement to another source, permission must also be sought from that source. If such permission is not obtained then that material may not be included in your publication/copies. Suitable acknowledgement to the source must be made, either as a footnote or in a reference list at the end of your publication, as follows:

"Reprinted from Publication title, Vol /edition number, Author(s), Title of article / title of chapter, Pages No., Copyright (Year), with permission from Elsevier [OR APPLICABLE SOCIETY

ELSEVIER LICENSE
TERMS AND CONDITIONS

Jul 01, 2011

This is a License Agreement between Samantha Smith ("You") and Elsevier ("Elsevier") provided by Copyright Clearance Center ("CCC"). The license consists of your order details, the terms and conditions provided by Elsevier, and the payment terms and conditions.

All payments must be made in full to CCC. For payment instructions, please see information listed at the bottom of this form.

Supplier	Elsevier Limited The Boulevard,Langford Lane Kidlington,Oxford,OX5 1GB,UK
Registered Company Number	1982084
Customer name	Samantha Smith
Customer address	311 Hunt Club Rd. Blacksburg, VA 24060
License number	2700031411020
License date	Jul 01, 2011
Licensed content publisher	Elsevier
Licensed content publication	Journal of the European Ceramic Society
Licensed content title	Opportunities of porous ceramics fabricated by gelcasting in mitigating environmental issues
Licensed content author	Minoru Takahashi, Ruben L. Menchavez, Masayoshi Fuji, Hiroaki Takegami
Licensed content date	March 2009
Licensed content volume number	29
Licensed content issue number	5
Number of pages	6
Start Page	823
End Page	828

Type of Use	reuse in a thesis/dissertation
Intended publisher of new work	other
Portion	figures/tables/illustrations
Number of figures/tables/illustrations	1
Format	both print and electronic
Are you the author of this Elsevier article?	No
Will you be translating?	No
Order reference number	
Title of your thesis/dissertation	Novel preparation of porous alumina using ice particles as pore-forming agents
Expected completion date	Jul 2011
Estimated size (number of pages)	75
Elsevier VAT number	GB 494 6272 12
Permissions price	0.00 USD
VAT/Local Sales Tax	0.0 USD / 0.0 GBP
Total	0.00 USD
Terms and Conditions	

INTRODUCTION

1. The publisher for this copyrighted material is Elsevier. By clicking "accept" in connection with completing this licensing transaction, you agree that the following terms and conditions apply to this transaction (along with the Billing and Payment terms and conditions established by Copyright Clearance Center, Inc. ("CCC"), at the time that you opened your Rightslink account and that are available at any time at http://myaccount.copyright.com).

GENERAL TERMS

2. Elsevier hereby grants you permission to reproduce the aforementioned material subject to the terms and conditions indicated.

3. Acknowledgement: If any part of the material to be used (for example, figures) has appeared in our publication with credit or acknowledgement to another source, permission must also be sought from that source. If such permission is not obtained then that material may not be included in your publication/copies. Suitable acknowledgement to the source must be made, either as a footnote or

A.2 International Union of Pure Applied Chemistry

From IUPAC website http://www.iupac.org/publications/pac/

IUPAC makes freely available the full texts of all articles published in *Pure and Applied Chemistry* on the IUPAC Web site, for all except the current and most recently completed volumes. In addition, authors may immediately deposit copies of their own articles online, for archival and distribution purposes, but only in the form of the IUPAC published pdf version. IUPAC Technical Reports and Recommendations are freely accessible from date of publication.

ISSN printed 0033-4545
ISSN electronic 1365-3075

Use of material such as figures and tables from articles published in *Pure and Applied Chemistry* is permitted so long as the source of the material is properly cited. If formal permission is required, please send a request to <pac@iupac.org>.